Monitoring Annual Forest Cover Fraction Change During 2000-2020 in China's Han River Basin Using Time-Series MODIS NDVI, VCF and Spatio-Temporal Regression

Xinyan Zhong, Yun Du, Xia Wang, Xiaodong Li, Wenqiong Zhao, Yihang Zhang, and Peter M. Atkinson

***Abstract*—While it is crucial to monitor the spatio-temporal dynamics of forests at the subpixel scale, most available nonlinear methods are used to predict forest cover fraction maps only at the acquisition time of the training samples and are, thus, unable to estimate time-series forest cover fraction beyond the acquisition time. Based on MODIS NDVI, VCF and Landsat tree canopy height data, we developed a spatio-temporal regression (STR) method to estimate annual forest cover fraction maps during 2000–2020 on China's Han River Basin. Results obtained by the proposed STR method achieved significantly higher accuracy ($R^2 = 0.897$, RMSE = 0.1364, MAE = 0.077) than that obtained by a traditional nonlinear regression method. Moreover, the STR exhibits increased accuracy when using training samples from both 2000 and 2020 compared to those using training samples solely from either 2000 or 2020. We also introduced Landsat tree cover maps in 2005, 2010, and 2015 as reference data to verify the effectiveness of the STR method. The STR method was employed to produce annual forest cover fraction maps from 2000 to 2020. The outcomes revealed a distinct overall recovery trend of forest cover at both the pixel and subpixel scales in China's Han River Basin during 2000–2020, notably around the vicinity of the Danjiangkou reservoir area. In general, the STR method proposed in this research is superior in accurately tracking time-series high-intensity and low-intensity forest cover fraction changes in a complex forest ecosystem, which is composed of various forest types in a subtropical monsoon climate.**

Manuscript received 29 March 2024; revised 31 May 2024; accepted 15 June 2024. Date of publication 21 June 2024; date of current version 12 July 2024. This work was supported in part by the National Natural Science Foundation of China under Grant 42271400 and Grant 62071457, in part by the Hubei Provincial Natural Science Foundation of China for Distinguished Young Scholars under Grant 2022CFA045, in part by the Key Research Program of Frontier Sciences, Chinese Academy of Sciences under Grant ZDBS-LY-DQC034, in part by the Young Top-notch Talent Cultivation Program of Hubei Province, and in part by the Yellow Crane Talent Program of Wuhan. *(Corresponding author: Yihang Zhang.)*

Xinyan Zhong and Wenqiong Zhao are with the Key Laboratory of Monitoring and Estimate for Environment and Disaster of Hubei Province, Innovation Academy for Precision Measurement Science and Technology, Chinese Academy of Sciences, Wuhan 430077, China, and also with the University of Chinese Academy of Sciences, Beijing 100049, China.

Yun Du, Xiaodong Li, and Yihang Zhang are with the Key Laboratory of Monitoring and Estimate for Environment and Disaster of Hubei Province, Innovation Academy for Precision Measurement Science and Technology, Chinese Academy of Sciences, Wuhan 430077, China (e-mail: zhangyihang@apm.ac.cn).

Xia Wang is with the CAS Key Laboratory of Aquatic Botany and Watershed Ecology, Wuhan Botanical Garden, Chinese Academy of Sciences, Wuhan 430074, China.

Peter M. Atkinson is with the Lancaster Environment Central, Faculty of Science and Technology, Lancaster University, LA1 4YQ Lancaster, U.K.

Digital Object Identifier 10.1109/JSTARS.2024.3417302

***Index Terms*—China's Han river basin, forest cover change, moderate resolution imaging spectroradiometer (MODIS), spatio-temporal regression (STR).**

I. Introduction

As ONE of the most important ecosystems on land, forests have crucial ecological functions, such as regulating climate, conserving water sources, and protecting biodiversity, while forests can also provide a series of forest by-products and create huge economic benefits for society [1], [2], [3]. However, forests constantly face the potential interference of natural and human factors. Despite the natural factors of fire, drought, and insect plague, the excessive deforestation caused by humans is the dominant driver of global forest loss, especially for the tropical forests [4], [5], [6], [7]. Therefore, effective monitoring and analysis of forest cover change is essential for the protection of Earth's remaining forests.

Remote sensing technology has the advantages of wide detection range, strong real-time performance, independence from ground conditions, and rich information acquisition, and it has been used widely for the monitoring of forest cover changes at both global and local scales [8], [9], [10]. Various remote sensing satellite sensor images have been applied to monitor forests, and these images have spatial resolutions ranging from the kilometer scale to meter scale.

Satellite sensor images with a spatial resolution of kilometers, such as NOAA-advanced very high-resolution radiometer (AVHRR) can capture phenological information about vegetation due to its fine temporal resolution, and it has been used widely for monitoring forests at a large scale. Jaramillo et al. [11] used NOAA-AVHRR images to evaluate the deforestation rate of El Guabo from 1986 to 2008. Lucas et al. [12] monitored the different stages of tropical forest regeneration in the Brazilian Amazon based on NOAA-AVHRR imagery. However, the coarse spatial resolution of NOAA-AVHRR makes it impossible to observe details of local forest cover with complex spatial patterns. In contrast, finer spatial resolution satellite sensor images such as Landsat, Sentinel-2, and Sentinel-1 can observe much more spatial details about the forest cover than kilometer-scale NOAA-AVHRR images. For example, Masek et al. [13] studied the trends of forest disturbances in the United States from 1985

to 2005 based on Landsat images. Frazier et al. [14] detected and quantified forest restoration in the Northern Shield ecoregion of Canada using time-series Landsat images. Reiche et al. [15] used Sentinel-1 SAR images to develop a tropical forest disturbance alert for the entire Congo Basin. Ganz et al. [16] mapped high-quality forest cover for the Baden-Württemberg area with Sentinel-2.

Satellite sensor images with very fine spatial resolutions, such as IKONOS, QuickBird, and WorldView-2, can also be used for the monitoring and analysis of forest cover changes. Zhu et al. [17] estimated the restored forest in semiarid mine dumps with WorldView-2 imagery. Wang et al. [18] compared the performance of QuickBird and IKONOS in mangrove classification. Although satellite sensor images with finer spatial resolutions have the ability to monitor more spatial details, their coarse temporal resolutions and narrow scanning width make it insufficient to meet the needs of monitoring complex forest landscapes in large areas. In addition, the relative long revisit periods of these fine spatial resolution satellite sensors also make the images more susceptible to cloud and fog.

Locating in the North–South climate transition zone of China, the Han River Basin is not only a key forest ecological area in China, but also the middle water supply route of the South-to-North water diversion project [19]. Long-term and effective spatio-temporal monitoring of forest cover changes in the Han River Basin is, therefore, desirable for better development and utilization of its ecological and economic resources. The Han River Basin holds extensive forest coverage and diverse forest types, such as evergreen forests coexisting with deciduous forests, coniferous forests, and broad-leaved forests [20]. Therefore, it would be more advantageous to monitor forest cover changes with complex landscapes and phenology in this region by using satellite sensor images with fine temporal resolution and large scanning width.

The moderate resolution imaging spectroradiometer (MODIS) images have a daily temporal resolution and long-term global data record since 2000, and it is able to capture seasonal vegetation phenology of complex forest landscapes in local and global scales. Moreover, compared to the kilometer-scale NOAA-AVHRR images, the hundred-meter MODIS images provide more detail on forest covers, which may be more suitable for monitoring and analyzing the complex forest landscapes in the Han River Basin. A series of product datasets has been developed for vegetation and forest changes monitoring by daily MODIS images, such as the widely used 16-days MODIS normalized difference vegetation index (NDVI) product. Based on MODIS NDVI, Singh et al. [21] used the breaks for additive seasonal and trend (BFAST) model to monitor forest disturbance frequency and disturbance scales in the Himalayas. Gao et al. [22] monitored subannual forest disturbance in the Mexican state of Michoacan with MODIS NDVI during 2000–2016. Yao et al. [23] applied MODIS NDVI data to study the response of forest cover dynamics to climate change from 2000 to 2009 in the Hun River Basin, Liaoning province of China. Through the integration of PALSAR and time series MODIS NDVI images during 2007–2010, Qin et al. [24] produced annual forest cover maps to monitor forest cover changes in South America.

Although the MODIS NDVI product has a finer spatial resolution than NOAA-AVHRR, it is still affected by mixed pixels when characterizing fragmented forest landscapes at the scale of hundreds of meters [25], [26]. To reduce the mixed pixels issues of MODIS NDVI, an alternative solution is to estimate MODIS forest cover fraction, which displays the surface forest cover at the subpixel scale [27], [28], [29], [30]. Traditional methods for estimating forest cover fractions include linear and nonlinear methods. Generally, linear decomposition cannot use the phenological information in time-series MODIS NDVI images [31], [32]. By contrast, nonlinear methods can estimate subpixel MODIS forest cover fraction from time-series MODIS NDVI. For example, Lu et al. [33] proposed a new approach to map fractional forest cover based on the combined use of MODIS data and Landsat images with linear spectral mixture analysis and regression model. Tottrup et al. [34] applied a supervised regression tree model to obtain fraction maps of mature forest, secondary forest, and nonforest from MODIS images. However, the nonlinear methods based on machine learning can process only single-phase forest cover fraction estimation at the acquisition time of the training samples [35]. Therefore, both the current linear and nonlinear methods cannot take full advantage of the long term-series MODIS NDVI and are inadequate for spatio-temporal estimation of forest cover fraction.

In addition to the MODIS NDVI, the MODIS vegetation continuous fields (VCF) provides the percentage of tree cover on the Earth's surface and can also be applied to monitor forest cover changes. Sarif et al. [36] used MODIS VCF data to monitor forest cover dynamics in Jharkhand from 2000 to 2014. Gao et al. [37] detected forest cover change in Mexico from 2000 to 2010 based on MODIS VCF. Hansen et al. [38] trained Landsat images with MODIS VCF to evaluate and analyze forest cover changes in the Congo during 1990–2000. Using Landsat images and MODIS VCF, Liu et al. [39] assessed three factors affecting Myanmar's forest cover change. However, the MODIS VCF product is based on the interannual periods, and then it is hard to consider the typical phenological changes of various complex forest landscapes in China's Han River Basin.

In this research, we proposed a spatio-temporal regression (STR) method to obtain annual forest cover fraction maps from 2000 to 2020 by integrating MODIS NDVI and VCF data and validated its performance through an application to China's Han River Basin. In the proposed STR method, time-series training samples can be predicted for each year from 2000 to 2020 by using a local change detection based on time-series MODIS VCF. The proposed method can not only make full use of the phenological information carried by MODIS NDVI data, but also be applied to the estimation of long time-series forest cover fraction. Based on the obtained time-series forest cover fraction maps, forest cover changes at the pixel and subpixel scales were monitored and analyzed.

The objectives of this article were as follows.

1) To develop a method and framework to estimate long-term annual forest cover fraction maps from MODIS NDVI and VCF with training samples at the start and end points;

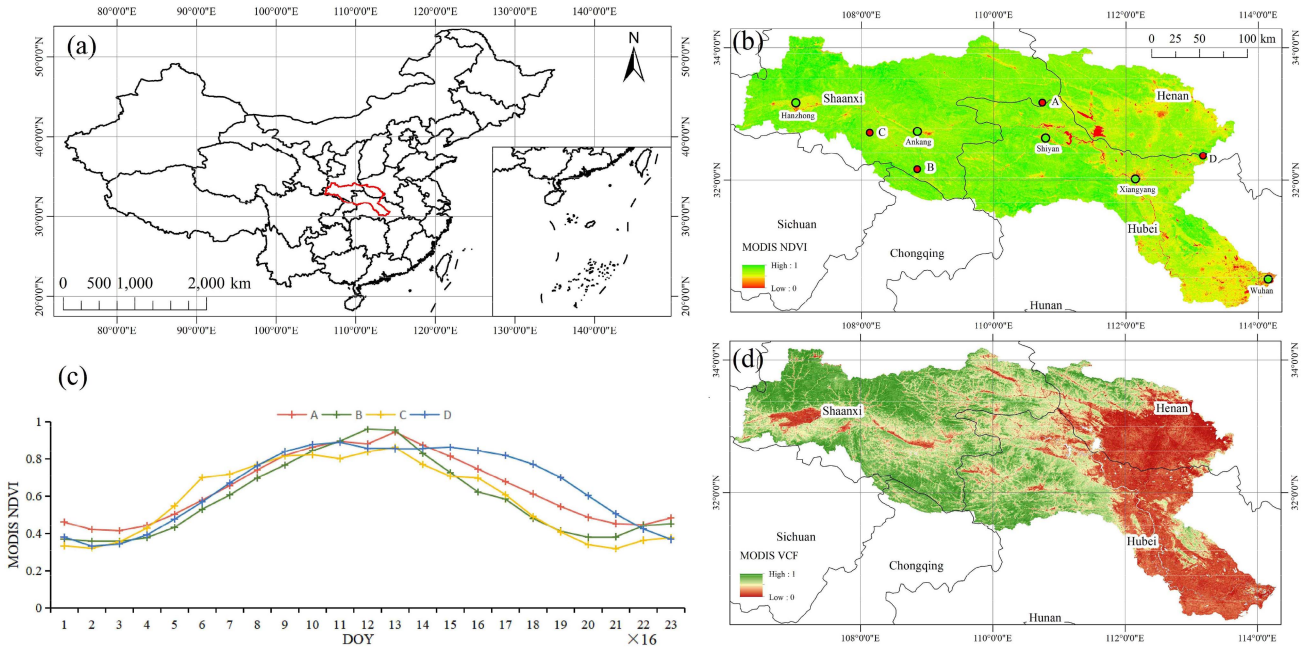

Fig. 1. Illustration of the study area and data sources. (a) Geolocation of China's Han River Basin. (b) Mean MODIS NDVI image in 2020. (c) Dynamic of time-series 16-day MODIS NDVI of four typical forest cover points in (b); (d) Percentage of tree cover layer of MODIS VCF image in 2020.

2) to improve the application of time-series MODIS NDVI and VCF data in mapping forest cover change across large regions;
3) to validate the performance of the proposed method in monitoring both high-intensity and low-intensity forest cover change in a complex forest ecosystem, such as the forests in China's Han River Basin within a subtropical monsoon climate.

The rest of this article is organized as follows. Section II describes the study area, data, and the preprocessing required. The principle and method of STR are introduced in Section III. Section IV presents and analyzes the prediction results obtained by the STR method, and provides a discussion of the performance of STR. Further discussion of the results as well as limitations and future research are summarized in Section V. Finally, Section VI concludes this article.

II. Study Area and Materials

A. Study Area

As one of the largest tributaries of the Yangtze River, China's Han River Basin has an area of 159 000 km^2 [20]. The Han River Basin is located in central China [see Fig. 1(a)], and covers five provinces of Henan, Hubei, Chongqing, Sichuan, Shaanxi, and Gansu in China. It has a mountain topography in the northwest (i.e., part of the Qinba Mountains) and plain hills (i.e., part of Jianghan Plain) in the southeast. The regional climate is mild and humid, belonging to the subtropical monsoon region. As shown in Fig. 1(b) and (c), most of the northwest mountains are covered by vegetation, and it is noted that the main land cover type in the area is forest, especially in the western mountains, where evergreen broadleaved forests, evergreen coniferous forests, deciduous broadleaved forests, deciduous coniferous forests, and mixed forests are distributed widely [19]. As the middle water source of the South-to-North Water Diversion Project, the Han River Basin has a high quality of ecological environment, and its rich forest resources and forest ecosystem can provide a strong guarantee for the water security of northern China.

B. Dataset and Preprocessing

As listed in Table I, in this study, three datasets (MODIS NDVI, MODIS VCF, and Landsat tree height) were used to estimate the annual 250 m fractional forest cover maps from 2000 to 2020 in China's Han River Basin. The collection and preprocessing (i.e., mosaic, clip, and projective transformation) of these three were completed on the platform Google Earth Engine.

The MODIS NDVI data used in this research come from the 250 m 16-day MODIS NDVI product of MOD13Q1, which has 23 corresponding NDVI time-series images each year, in which the NDVI value of each pixel is the optimal value of the corresponding 16 days. The time-series 16-day MODIS NDVI has a fine temporal resolution and holds the advantage of preserving well the phenological information of vegetation [40], [41]. However, due to the influence of inevitable cloud cover, there will be many outliers in the final MODIS NDVI product, which will introduce noise into the normal NDVI trend of vegetation. NDVI reconstruction (spatio-temporal filtering) methods can be used to reduce or eliminate the effects of MODIS NDVI outliers [42], [43]. In this study, the Savitzky–Golay filter [44], [45] was used to reconstruct spatio-temporal smoothed NDVI for annual 250 m 16-day MODIS NDVI images. The

TABLE I
SUMMARY OF DATASETS USED IN THIS STUDY

Name	Product	Spatial resolution (m)	Temporal resolution	Period	Dataset Provider
MODIS NDVI	MOD13Q1.061	250	Every 16-day	2000–2020	NASA LP DAAC at the USGS EROS Center
MODIS VCF	MOD44B.006	250	annual	2000–2020	NASA LP DAAC at the USGS EROS Center
Landsat tree canopy Height	GLAD Global Forest Canopy Height dataset	30	1-year	2000, 2019, 2020	University of Maryland
Global Forest Cover Change (GFCC)	Tree Cover MultiYear Global	30	Every 5-year	2000, 2005, 2010, 2015	NASA LP DAAC at the USGS EROS Center

Savitzky–Golay filter was applied to the annual 16-day MODIS NDVI images using a plug-in in ENVI. To ensure that the initial and final 16-day MODIS NDVI images of each year were smoothed successfully by the Savitzky–Golay filter with a width of 5 pixels, another four images were added at the beginning and end of each year. The first four images are from the end of the previous year, and the last four images are from the beginning of the following year.

The MODIS VCF data were derived from the annual 250 m MODIS VCF product of MOD44B, which provides the percentage of tree cover layer at the global scale since 2000. In the MOD44B product, the layer, percent tree cover, indicates the area covered by trees with a canopy height greater than 5 m in the corresponding year [46]. Based on a supervised regression tree model, the product is generated from a yearly composite of MODIS 16-day surface reflectance including bands 1–7 and brightness temperature bands, in which the reference samples were collected from a number of downsampled Landsat-based land cover maps [47]. Given the superiority of presenting yearly forest canopy dynamics, MODIS VCF data have been used widely to monitor forest cover change at both local and global scales [48], [49], and they were also considered as the input data for this research.

Based on a bagged regression trees ensemble method, the 2019 forest height map was derived from the integration of GEDI-derived canopy height indicators with Landsat multitemporal surface reflectance data.[1] Vegetation structure data collected using airborne lidar instruments has been used for model calibration and validation of the generated forest height [50]. The 2000 and 2020 tree canopy height maps used in this research were extracted from the GLAD Global Land Cover and Land Use Change dataset.[2] This dataset was compiled from a survey of Global Ecosystem Dynamics Investigation (GEDI),[3] with Landsat multitemporal surface reflectance data [51]. Although tree canopy height in 2019 was produced first, 2000 and 2020 tree canopy height maps were produced in the same way for 2019, making these data consistent across the three periods. The three Landsat tree canopy height maps will be used to generate binary forest cover maps and the corresponding MODIS-like forest cover fraction maps in 2000, 2019, and 2020.

As shown in Table I, the GFCC product was estimated from the global land survey data, which provides the global composite 30 m Landsat images at years of 2000, 2005, 2010, and 2015. For each pixel in GFCC, it provides the percentage of tree cover at 5-year epochs [52], [53]. In this study, this data will be used to generate MODIS-like forest cover fraction maps in 2005, 2010, and 2015. The forest cover fraction maps obtained in these three years will serve as another set of reference data for accuracy assessment and comparison.

III. METHODS

Based on the time-series MODIS NDVI and VCF input data, and time-series training samples extracted from the Landsat tree canopy height maps in 2000 and 2020, the aim was to predict annual 250 m annual fractional forest cover maps during 2000–2020 using the proposed STR model. As illustrated in Fig. 2, the methods of this research can be divided generally into three steps as follows:

1) Processing input data;
2) modeling STR;
3) estimating and validating annual fractional forest cover maps from 2000 to 2020.

The input data processing was completed in the above Section II-B. More details about the last two steps can be found in the following sections.

A. Spatio-Temporal Regression

As the key part of the proposed method, STR aims to estimate forest fractional forest cover from the MODIS NDVI sequence and VCF images at the predicting year from 2000 to 2020. The STR model includes the following three steps:

[1]Data is available online at: https://glad.umd.edu/dataset/gedi/
[2]Data is available online at: https://glad.geog.umd.edu/dataset/GLCLUC2020
[3]Data is available online at: https://gedi.umd.edu/

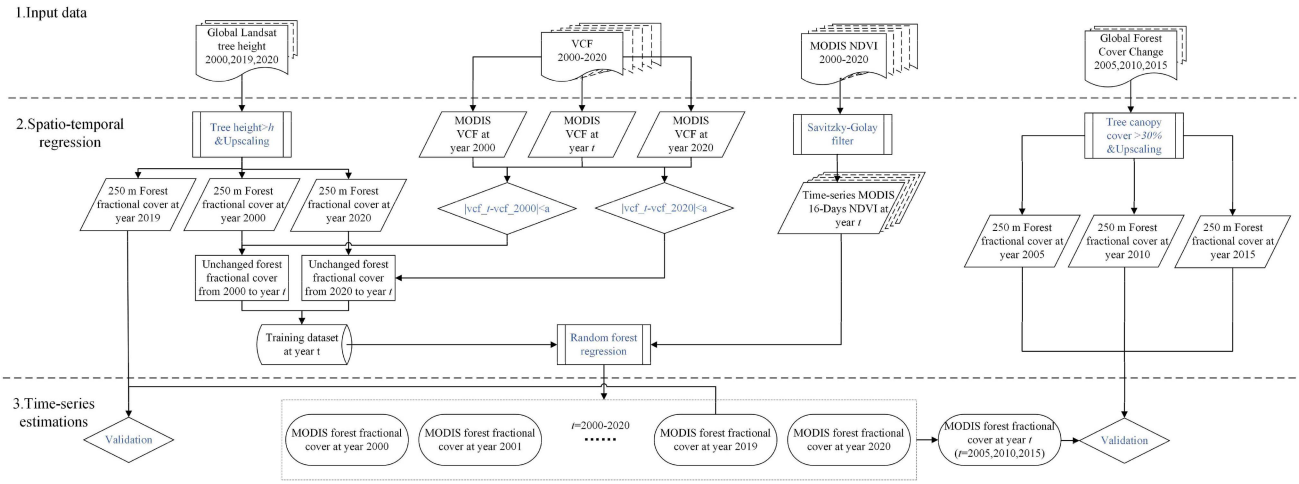

Fig. 2. Proposed methodology.

1) Generate reference MODIS-like forest cover fraction maps;
2) unchanged training samples selection in each predicted year;
3) estimate forest cover fraction maps with random forest (RF) regression and time-series samples.

B. Reference MODIS-Like Forest Cover Fraction Maps

By processing the Landsat tree canopy height data in 2000, 2019, and 2020, the forest cover fraction maps of the corresponding years can be obtained. This process includes the two steps:

1) Generation of Landsat binary forest cover maps. According to Potapov et al. (2022) [51], land cover featuring a canopy height exceeding 5 m is commonly classified as forested area. Consequently, pixels displaying a value greater than or equal to 5 m in the tree height dataset are designated as forest pixels and coded as "1." Conversely, nonforest pixels are attributed a value of "0." Subsequently, this process yields a binary forest cover map for the specific year, possessing a spatial resolution of 30 m. To further validate the accuracies of the generated 30 m binary forest cover maps in 2000 and 2020, we collected 200 sample points for each of the forest cover and the nonforest cover in the two years, respectively. Based on the yearly composite Landsat images in 2000 and 2020, visual interpretation method was used to determine the reference classes of each sample points. Finally, the confusion matrixes were calculated and the overall accuracy of the binary forest cover map for 2000 is 0.9625, and the kappa coefficient is 0.925. For the binary forest cover map in 2020, the overall accuracy and kappa coefficient are 0.9575 and 0.915, respectively.
2) Prediction of MODIS-like forest cover fraction maps. The obtained Landsat forest cover maps were first downsampled to 240 m with a spatial averaging filter of 8×8 pixels, and then the forest cover fraction maps with a spatial resolution of 250 m in the corresponding years of 2000, 2019, and 2020 were derived by downsampling the 240 m forest cover fraction maps using a nearest neighbor interpolation. The resulting 250 m forest cover fraction maps for 2000 and 2020 were used to build the training dataset needed for subsequent estimations, and the forest cover fraction map for 2019 served as validation data.

C. Unchanged Time-Series Training Samples Selection

In Section III-B, we obtained the forest cover fraction for 2000 and 2020, which can be used to construct a training dataset in these two years with the corresponding MODIS NDVI sequence and VCF images. Given the missing forest cover fraction of 2001–2019, it is easy to estimate the time-series annual forest cover fraction maps during 2001–2019 using the training samples in 2000 and 2020. However, due to varying external environmental conditions (such as temperature and precipitation) in each year during 2000–2020, the trained models in 2000 and 2020 can estimate only the forest cover fraction of the current year well, and it is inevitable that there will be large errors in estimation for the other years during 2001–2019.

Considering that MODIS VCF data contain spatial and temporal information on forest cover change [48], [53], [54], the change detection method based on MODIS VCF is used here to obtain annual training samples during 2001–2019 from the original training samples in 2000 and 2020. MODIS VCF provides the percentage of tree cover: When the difference between the percentage tree cover values in a target pixel for a certain two years is less than a given threshold, we can assume that the forest cover in this pixel is similar between these two years, and this target pixel can be considered a constant pixel. However, MODIS VCF data may have abnormal pixel values due to the influence of inevitable cloud cover. In this case, if only the difference between the percentage tree cover of the target pixel for two years is used to determine whether it is a constant pixel, the judgment may be affected seriously by outliers. Therefore, instead of using the single target pixel, its neighboring pixels

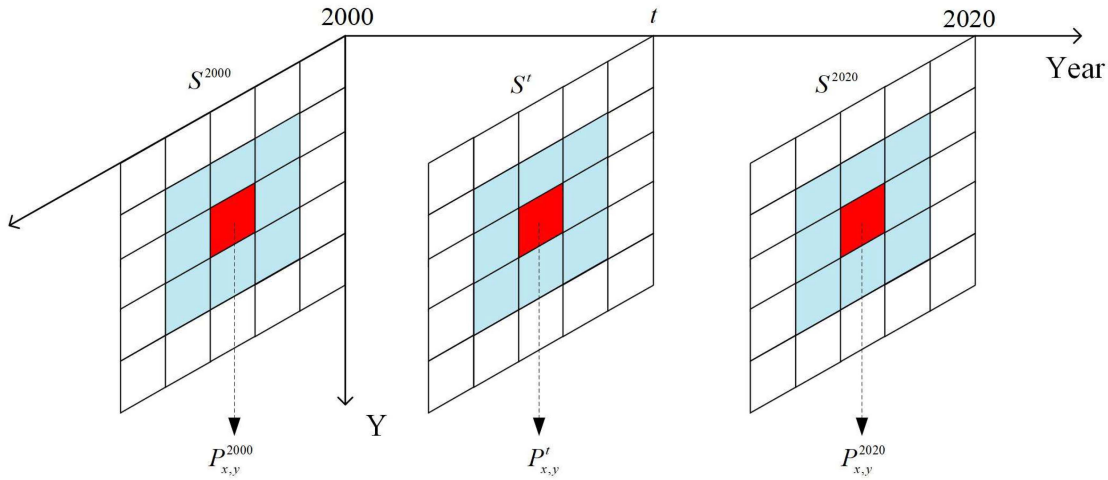

Fig. 3. Illustration of change detection for time-series training samples with a 3 × 3 neighborhood window system.

can be introduced to build a neighborhood window system, to indicate the change in percentage tree cover between two years.

As shown in Fig. 3, S^{2000}, S^{2020}, and S^{t} are samples from year 2000, 2020, and t, respectively. When selecting training samples, threshold a should be set first. The target pixel can then be considered as a constant pixel when its difference between the corresponding pixels in 2000 and 2020 are less than the given threshold a. Based on the constant pixel, the training sample $S^{t}_{x,y}$ can be selected from $S^{2000}_{x,y}$ and $S^{2020}_{x,y}$ with the following:

$$S^{t}_{x,y} = \begin{cases} S^{2000}_{x,y} & if \left|\bar{p}^{t}_{x,y} - \bar{p}^{2000}_{x,y}\right| < a \\ S^{2020}_{x,y} & if \left|\bar{p}^{t}_{x,y} - \bar{p}^{2020}_{x,y}\right| < a \end{cases}$$
$$t \in [2000, 2001, \cdots, 2020] \quad (1)$$

$$\bar{p}^{t}_{x,y} = \frac{1}{w \times w} \sum_{n=1}^{w \times w} P^{t}_{x,y}(n) \quad (2)$$

where $P^{t}_{x,y}$ is the target pixel value in MODIS VCF image in year t (red tone pixel in Fig. 3), and $P^{2000}_{x,y}$ and $P^{2020}_{x,y}$ are the corresponding pixels in MODIS VCF images in 2000 and 2020. $\bar{p}^{t}_{x,y}$, and $\bar{p}^{2020}_{x,y}$ are mean pixel values of the neighborhood windows for each of the target pixels, and they can be calculated with (2). The neighborhood window system is composed of $w \times w$ pixels centered at target pixels of $P^{t}_{x,y}$, $P^{2000}_{x,y}$, and $P^{2020}_{x,y}$ (w is 3 in this study). A training sample dataset of $\{S^{t}_{x,y}, t \in [2000, \ldots, 2020]\}$ at each of the predicting years during 2000–2020 can be obtained based on the above change detection shown in (1) and (2). Ideally, the closer the value of a is to 0, the higher the quality of the obtained samples, but this will result in a smaller number of samples in the training dataset. Therefore, a value of $a = 0.1$ was chosen to provide sufficient high-quality training samples.

D. RF Regression With Time-Series Samples

With the above training samples $\{S^{t}_{x,y}, t \in [2000, \ldots, 2020]\}$ for each year from 2000 to 2020, the forest cover fraction map for each year during 2000–2020 can be estimated using RF regression. The RF regression model takes the 16-day MODIS NDVI sequence and annual MODIS VCF value for each year as input, and the corresponding MODIS-like forest cover fraction value in the selected training samples as the output. RF is an ensemble and learning algorithm based on decision trees, classification and regression tree (CART), which selects randomly n samples from n training samples to obtain m subsets (Di) by bootstrap sampling method, and trains a decision tree (Ti) for each subset separately, and takes the average of the prediction results (Ci) of m decision trees as the output of the RF regression [55], [56]. The RF simplified formula is as follows:

$$C = \frac{1}{m} \sum_{i=1}^{m} C_i \quad (3)$$

The RF algorithm is relatively stable and reduces the risk of overfitting by averaging the decision tree [57], [58]. Therefore, it is suitable for the estimation of forest cover fraction in this research. Estimation using RFs often involves the selection of model parameters (number of decision trees, etc.). The decision tree number was set to 100, and other parameters were set by default. After fitting the training samples with RF regression, the MODIS NDVI sequence, and annual MODIS VCF images for each year during 2001–2020 can be used finally for the model to predict the annual forest fraction maps.

E. Accuracy Assessment and Comparison

In the above Section III-B, a forest cover fraction map with a spatial resolution of 250 m in 2019 was obtained, which can be used as a reference map to evaluate the accuracy of the results estimated by different methods. Specially, for the proposed STR method, unchanged training samples for 2019 can be detected first from the reference forest fraction maps of 2000, 2020, or both 2000 and 2020 with (1), and the 250 m forest cover fraction maps in 2019 can be estimated with these unchanged samples. For traditional nonlinear regression method, the forest cover fraction map with a spatial resolution of 250 m in 2019 can also be estimated using a with training samples in the forest fraction maps of 2000 and 2020. When conducting accuracy assessment and comparison, we adopted two strategies: the first is based on

TABLE II
ACCURACY ASSESSMENT AND COMPARISON OF THE TENFOLD CROSS VALIDATION FOR THE RESULTS IN 2019 GENERATED BY THE PROPOSED STR METHOD AND TRADITIONAL RF METHOD

Samples collection year	R^2		*RMSE*		*MAE*	
	RF	STR	RF	STR	RF	STR
2000	0.779±0.0188	0.887±0.0093	0.2435±0.0134	0.1457±0.0067	0.1491±0.0092	0.0802±0.0039
2020	0.888±0.0142	0.908±0.0141	0.1494±0.0076	0.1275±0.0085	0.1031±0.0056	0.073±0.0046
2000+2020	0.845±0.006	0.909±0.0056	0.1792±0.0036	0.1295±0.0033	0.1161±0.0029	0.072±0.0016

the tenfold cross validation, in which it aims to randomly select 90% of the samples as training data and 10% as validation data; the second is to use all samples for training and, then, evaluate and compare the results with reference data in the other years of 2019 (i.e., extracted from Landsat tree height map), 2005, 2010, and 2015 (i.e., extracted from GFCC tree canopy cover).

The accuracy of results was evaluated using the following metrics:

$$RMSE = \sqrt{\frac{\sum_{i=1}^{n}(r_1-p_1)^2+\cdots+(r_i-p_i)^2+\cdots+(r_n-p_n)^2}{n}} \tag{4}$$

$$MAE = \frac{1}{n}\sum_{i=1}^{n}|(r_1-p_1)|+\cdots+|(r_i-p_i)|+\cdots+|(r_n-p_n)| \tag{5}$$

$$R^2 = \frac{\sum_{i=1}^{n}(r_i-\bar{r})^2-\sum_{i=1}^{n}(r_i-p_i)^2}{\sum_{i=1}^{n}(r_i-\bar{r})^2} \tag{6}$$

where n is the number of validation samples, r_i is the reference forest cover fraction of the ith sample, p_i is the predicted forest cover fraction for the ith sample, $\bar{r}$ is the average of the reference forest cover fraction of the n validation samples. Specially, 5000 samples were used for accuracy assessment and validation, and they were extracted randomly from the reference forest cover fraction map in 2019.

In addition to using the forest cover fraction map obtained from the Landsat tree canopy height data in 2019 as reference data, we also introduced GFCC data to more rigorously verify the effectiveness of the proposed method. The tree canopy cover of GFCC was segmented with 30% as the threshold to obtain the binary forest cover maps, and then the 250 m forest cover fraction maps corresponding to 2005, 2010, and 2015 were obtained by spatially average filtering of the 30 m binary forest cover maps. Similarly, 5000 points were randomly selected from each year for accuracy assessment and compare.

IV. EXPERIMENTAL RESULTS

A. Forest Cover Fraction Map Estimation in 2019

In this section, the fraction cover map in 2019 was selected as the reference for comparing results estimated by the STR method and the traditional nonlinear RF regression method. For the STR method and the traditional nonlinear RF regression method, training samples from 2000, 2020, and both 2000 and 2020 were used to predict cover fraction maps from the 16-day MODIS NDVI sequence and annual MODIS VCF images in 2019, respectively. The tenfold cross validation for the results in 2019 are shown in Table II. Moreover, the accuracy assessment and comparison using all training samples are shown in Table III and the corresponding accuracy assessment based on the scatterplots is depicted in Fig. 4. By using the forest cover fraction maps generated from GFCC as reference data, Table IV shows the accuracy assessment and comparison in the validation years of 2005, 2010, and 2015 for results generated by the proposed STR method with the combined samples of 2000 and 2020. By observing Tables II–IV, it can be found that the proposed STR method can obtain more accurate fraction cover maps than the traditional RF method with different reference validation data.

Forest cover fraction maps generated from STR by using all training samples and the corresponding difference maps between the predicted and reference forest cover fraction maps are illustrated in Fig. 5, in which the area of Hanzhong city is selected as the zoomed area. Looking at Fig. 5, when the traditional RF method was used, the forest cover fraction values in the result obtained from the samples in 2000 are generally higher than those in the reference map [see Fig. 5(a)], and the regions with large negative difference (i.e., error) values are distributed in the western, central, and southeastern parts of the study area, especially in the southeastern part [see Fig. 5(d)]. This means that the overestimation is serious. The prediction result obtained from the samples in 2020 is generally lower than the reference result [see Fig. 5(b)], in which the regions with large positive difference are distributed in the western, central, and northern parts of the study area [see Fig. 5(e)]. This means that the underestimation is serious. After combining the samples in 2000 and 2020, as shown in Fig. 5(c), the predicted result visually improved greatly, in which the numbers of large positive and negative values in the difference map [see Fig. 5(f)] are much smaller than those based on samples in 2000 and 2020. However, there are still significant differences between the estimated values and the reference values in the western and southeastern regions of the Han River Basin. The reason behind this is that the external environmental conditions are different in each year, and the same pixel with similar NDVI sequences in different years may correspond to different forest cover fraction values, so that the samples obtained by the traditional RF method can predict only the forest cover fraction of the current year. For example, if the forest cover fraction values for samples in 2000 all stay at a low level, the results obtained by the traditional RF method and the samples of 2000 will also stay at a lower level than the reference value.

TABLE III
ACCURACY ASSESSMENT AND COMPARISON OF THE RESULTS IN 2019 GENERATED BY THE PROPOSED STR METHOD AND TRADITIONAL RF METHOD (USING ALL SAMPLES)

Samples collection year	R^2		*RMSE*		*MAE*	
	RF	STR	RF	STR	RF	STR
2000	0.792	0.892	0.2215	0.1393	0.1292	0.077
2020	0.87	0.895	0.1621	0.1379	0.1121	0.079
2000+2020	0.851	0.897	0.1657	0.1364	0.1079	0.077

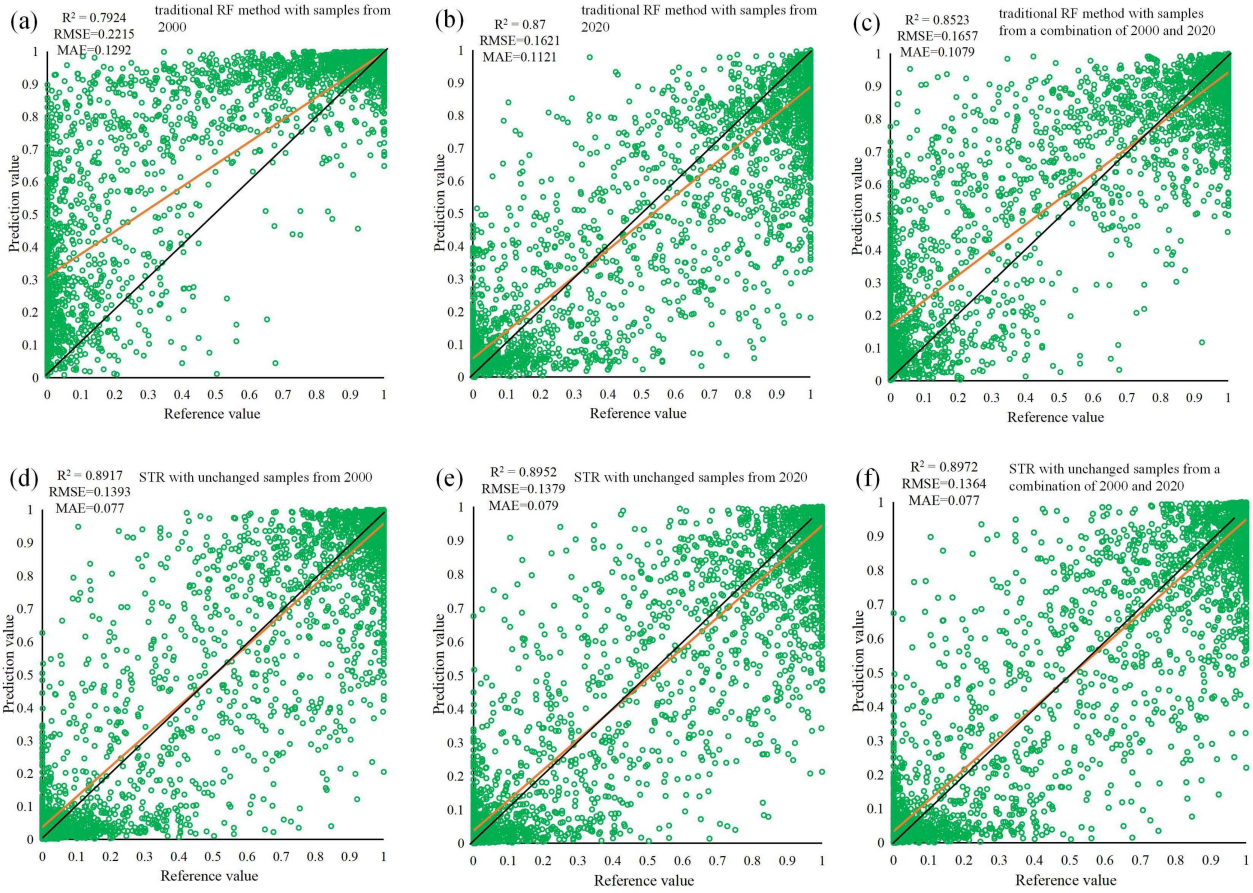

Fig. 4. Scatter plots between the estimated forest cover fraction values for the year of 2019 and reference values based on the validation samples in 2019. (a), (b), (c) Scatter plots for the forest cover fraction values in 2019 estimated by the traditional RF method with samples in 2000, 2020, and a combination of 2000 and 2020, respectively. (d), (e), (f) Scatter plots for the forest cover fraction values in 2019 estimated by the proposed STR with unchanged samples selected from 2000, 2020, and a combination of 2000 and 2020, respectively.

TABLE IV
ACCURACY ASSESSMENT AND COMPARISON IN THE VALIDATION YEARS OF 2005, 2010, AND 2015 FOR RESULTS GENERATED BY THE PROPOSED STR METHOD WITH THE COMBINED SAMPLES OF 2000 AND 2020 (FOREST COVER FRACTION MAPS GENERATED FROM GFCC WERE USED AS REFERENCE DATA)

Validation year	R^2		*RMSE*		*MAE*	
	RF	STR	RF	STR	RF	STR
2005	0.66	0.72	0.3185	0.2846	0.2193	0.1775
2010	0.646	0.755	0.2846	0.2292	0.19	0.1367
2015	0.804	0.888	0.2283	0.1601	0.1324	0.0846

As shown in Fig. 5(g)–(i), after using the proposed STR method, the above problems are well solved. Comparing the Fig. 5(g)–(i) and (m), it is found that the three results are more similar to the reference forest cover fraction map in the whole study area than the results obtained by the traditional RF method. Through the difference maps of the three results [see Fig. 5(j)–(l)], it can also be found that the overestimation and underestimation against the reference values in the results of the traditional RF method have also been significantly reduced in the results of the proposed STR method, especially in the northern region and the southeast region.

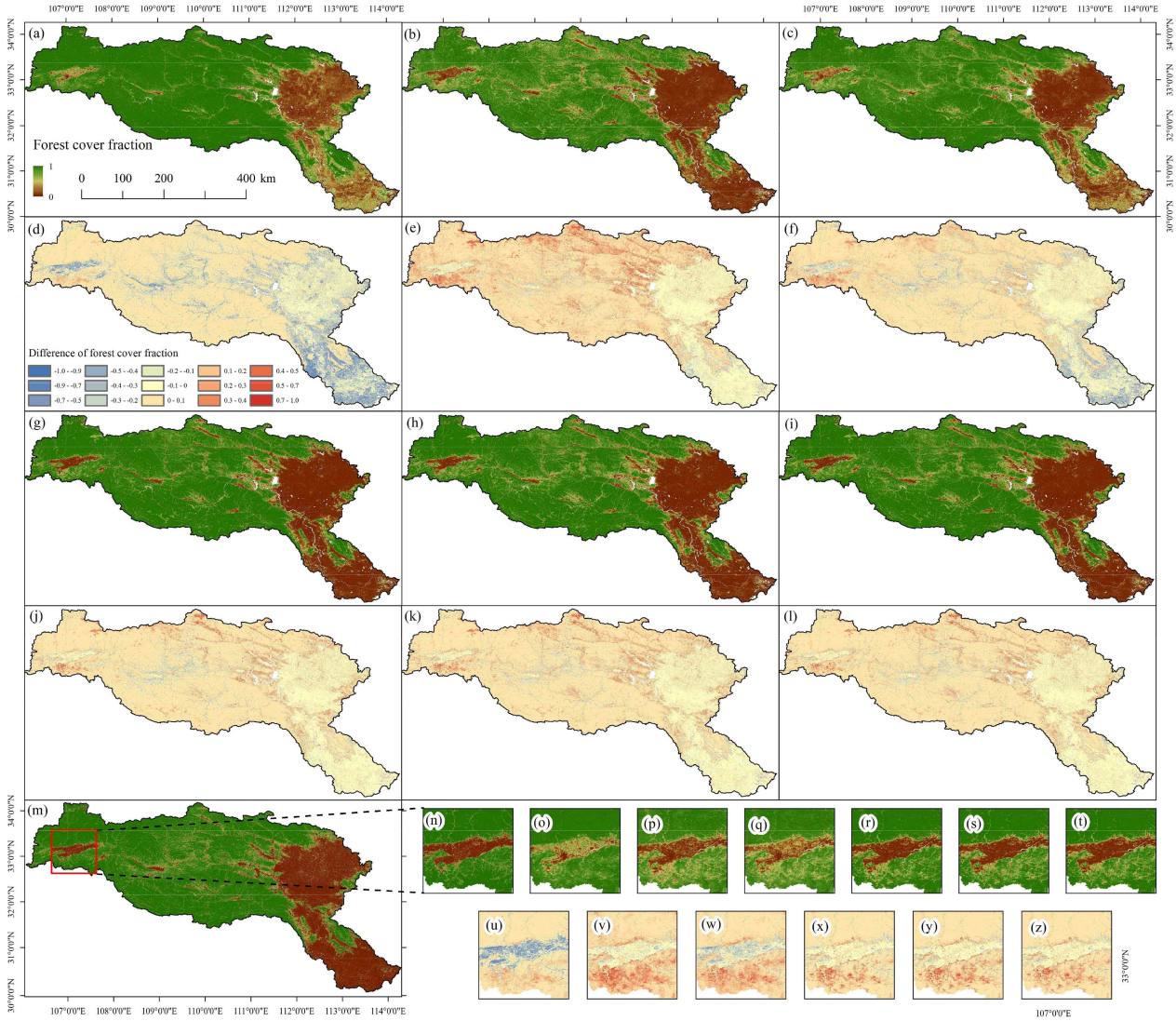

Fig. 5. Forest cover fraction maps and corresponding error maps with a spatial resolution of 250 m obtained by different methods. (a)–(c) Forest cover fraction maps in 2019 estimated by the traditional RF method with samples in 2000, 2020, and a combination of 2000 and 2020, respectively. (d)–(f) Difference (error) maps between the prediction results of (a)–(c) and the reference map in (m). (g)–(i) Forest cover fraction values in 2019 estimated by the proposed STR with unchanged samples selected from 2000, 2020, and a combination of 2000 and 2020, respectively. (j)–(l) Difference (error) maps between the results of (g)–(i) and the reference map in (m). (m) Reference forest cover fraction map in 2019. (n) Zoomed area of (m). (o)–(q) Zoomed areas of (a)–(c). (r)–(t) Zoomed areas of (g)–(i). (u)–(w) Zoomed areas of (d)–(f). (x)–(z) Zoomed areas of (j)–(l).

The area near Hanzhong city is taken as an example for the zoomed area analysis and comparison [see Fig. 5(n)-(t)]. When using the traditional RF method, the result [see Fig. 5(o)] obtained from the sample from 2000 presents significantly higher forest cover fraction values than the reference [see Fig. 5(n)] throughout the region, and the boundaries between many forest and nonforest areas are not clear. The fraction values in the result based on the samples in 2020 are more accurate than for 2000, but the forest texture is still blurred [see Fig. 5(p)]. The result obtained by combining the samples of 2000 and 2020 also produces many overestimated or underestimated prediction values in the whole region [see Fig. 5(w)]. After using the STR method, it can be found that the results depict more texture details [see Fig. 5(r)–(t)] of forests, and the deviation of the prediction values is also significantly reduced [see Fig. 5(x)–(z)], leading to more accurate reflection of the real spatial distribution of forest cover in the region. In addition, when taking samples from 2000 as an example, the accuracy obtained by the STR method is significantly increased compared to the traditional RF method (see Table III), and only slightly inferior to that of the year of 2020, which demonstrates that the STR method can provide more accurate and stable estimation of forest cover fraction when making long-time series predictions.

B. Annual Forest Cover Fraction Map Estimation From 2000 to 2020

This section obtains the annual forest cover fraction maps for each year from 2000 to 2020 in the Han River Basin, and the results are depicted in Fig. 6. Using STR method,

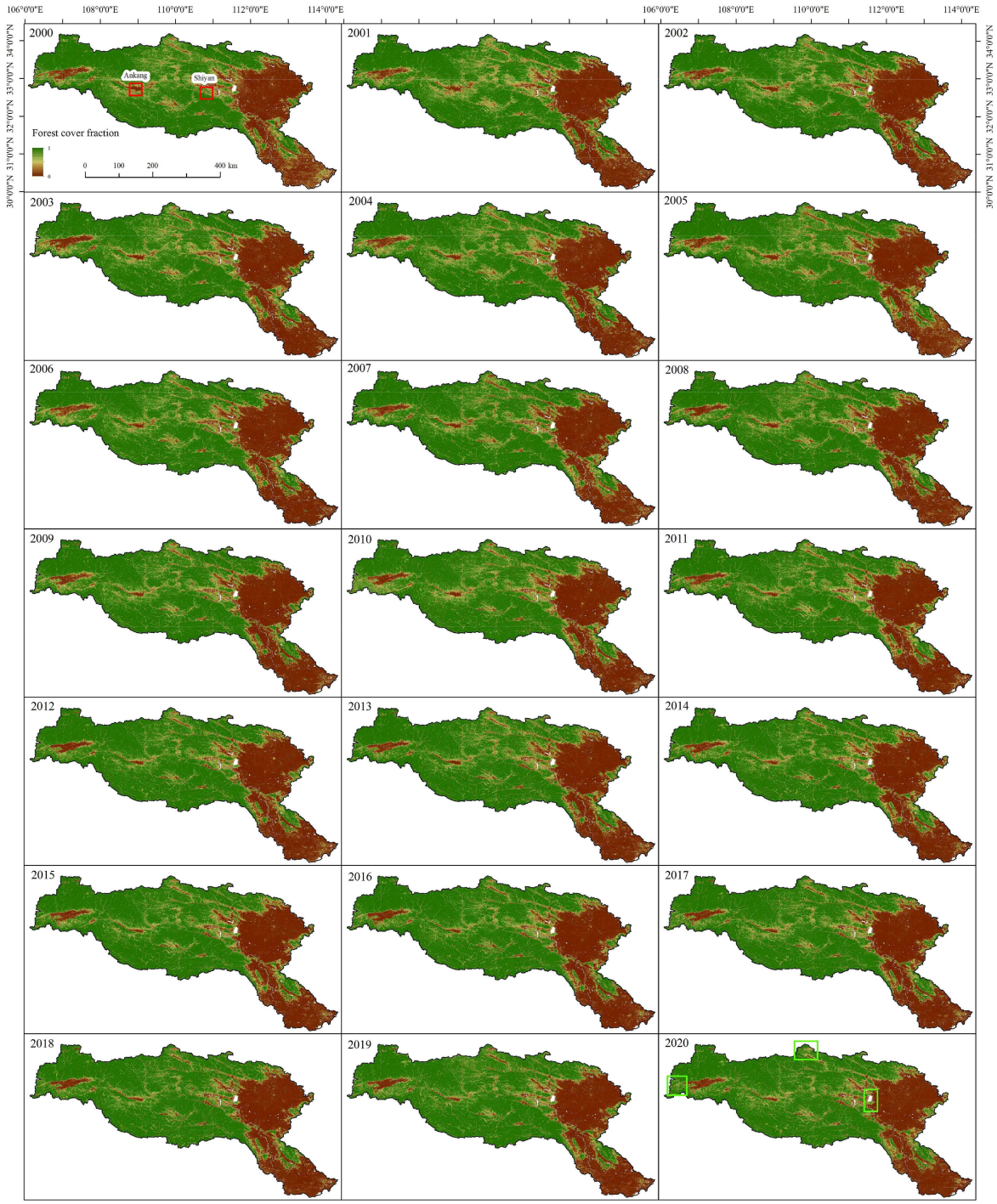

Fig. 6. Annual 250 m forest cover fraction maps in China's Han River Basin during the period from 2000 to 2020 estimated by the proposed STR method. The areas in the red box are further discussed and analyzed in 4.2.1 and 4.2.2 as typical areas of forest increase and decrease.

the corresponding time-series samples for each year during 2000–2020 were obtained based on the reference forest cover fraction maps of 2000 and 2020, and the model for each year was constructed and trained with the selected unchanged samples at the predicting year. The 16-day MODIS NDVI sequence and annual MODIS VCF images in the predicting year were used as the input of the predicting model to obtain the forest cover fraction map.

As shown in Fig. 6, it is clear that significant forest recovery occurred from 2000 to 2020 in China's Han River Basin, especially in the central region, such as Ankang City, Shaanxi Province (see Ankang in Fig. 6). Moreover, obvious forest recovery also occurred around Hanzhong City, Shaanxi Province, as well as the forests in Shangluo City, Shaanxi Province and the Danjiangkou Reservoir area in eastern Hubei Province (see green boxes in Fig. 6). The remarkable restoration of forests in

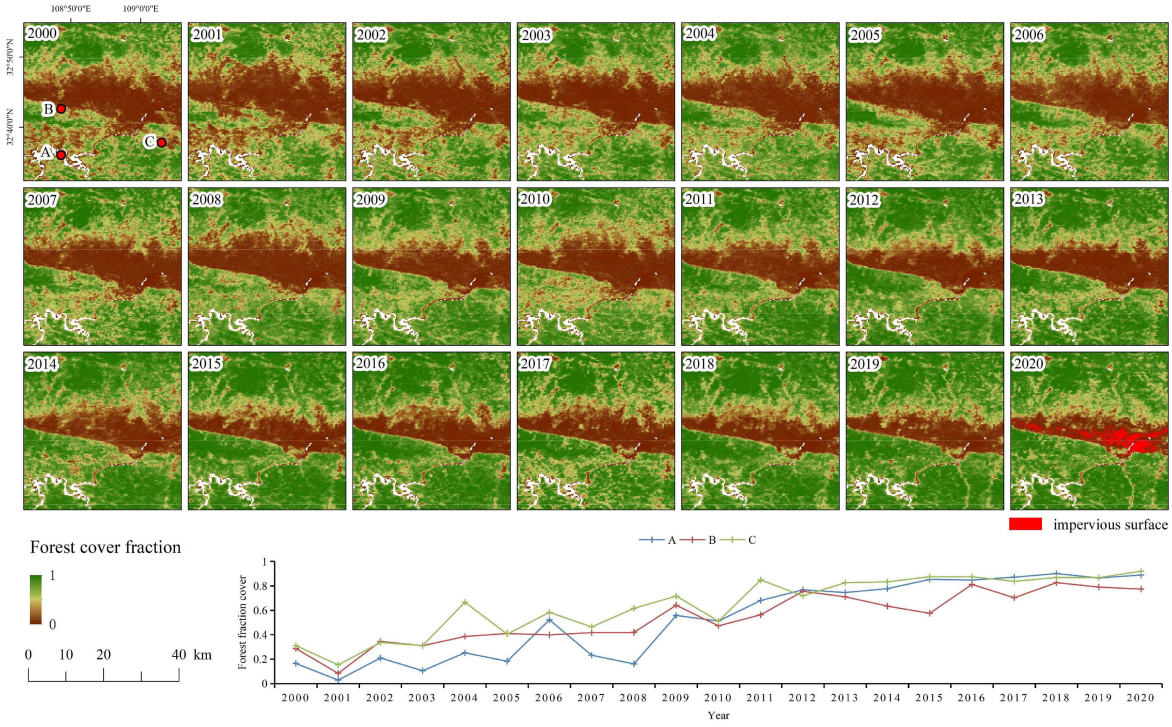

Fig. 7. Estimated annual forest cover fraction maps for the typical area of forest growth in Ankang City, Shaanxi Province.

these regions is a testament to the effectiveness of the Chinese government's forest conservation policies. However, there were also some areas that experienced forest fraction decline during the study period (see Shiyan in Fig. 6), which may be related to the development and construction of rapid urban expansion during the past two decades.

C. Illustration of Forest Cover Fraction Increases During 2000–2020

Ankang City, located in the southeast of Shaanxi Province, was selected as a typical area of forest restoration in the study area for further analysis (see Fig. 7). From the results, the forest cover fraction in Ankang City showed a year-by-year increasing trend from 2000 to 2020, and the forest cover fraction with high values expanded significantly. In particular, the restoration of the forest in the northern part of Ankang City is more obvious than other places, and the northern forest fractions were expanding to the city year by year. The forests in the southern part of Ankang City also showed an obvious recovery process, and the forest cover fraction of many sparse forests increased significantly, indicating an increasing densityof forests. For example, the forest cover fraction values of the three indicator points selected around Ankang City changed from low values at the beginning to high values after a series of fluctuations, indicating that forests in these areas were well restored under the forest protection policies, such as returning farmland and grassland to forest as promoted by the Chinese government. Furthermore, by comparing with the impervious surface area (see 2020 in Fig. 7), it can be found that the increase in forest occurred mainly around the urban area, which indicates that Ankang City attached great importance to the protection of the ecological environment around the city in the process of development.

D. Illustration of Forest Cover Fraction Decreases During 2000–2020

Shiyan City was selected as a typical area of forest decrease for further analysis. As shown in Fig. 8, the forest cover fraction in Shiyan urban area exhibited a year-by-year downward trend from 2000 to 2020. For example, the forest cover fraction values of the three indicator points located around Shiyan City experienced a series of fluctuations from the high value at the beginning to a low value at the end year of 2020 (see Fig. 8). Compared to the impervious surface area shown in Fig. 8, it can be found that the forest decreases in the city of Shiyan, and even the forest in the northwest and northeast around Shiyan city, experienced an obvious increase. As a representative large city in the northwest of Hubei Province, Shiyan City is also an important transportation hub in Hubei Province, with a relatively complete industrial system. In the process of city development during the past two decades, due to the adjustment of industrial structure and the influx of a large number of migrant populations, Shiyan City has developed and utilized a large number of urban internal spaces during the study period, which has led to a decrease in forested area in the city. On the other hand, as in the vicinity of Ankang City, forest cover fraction in many parts of Shiyan also shows an increasing trend, such as in the northern, northwestern, and eastern parts. It shows that in the past 20 years, although Shiyan city has experienced a decline in forests in the city due to rapid urban development, the forest cover

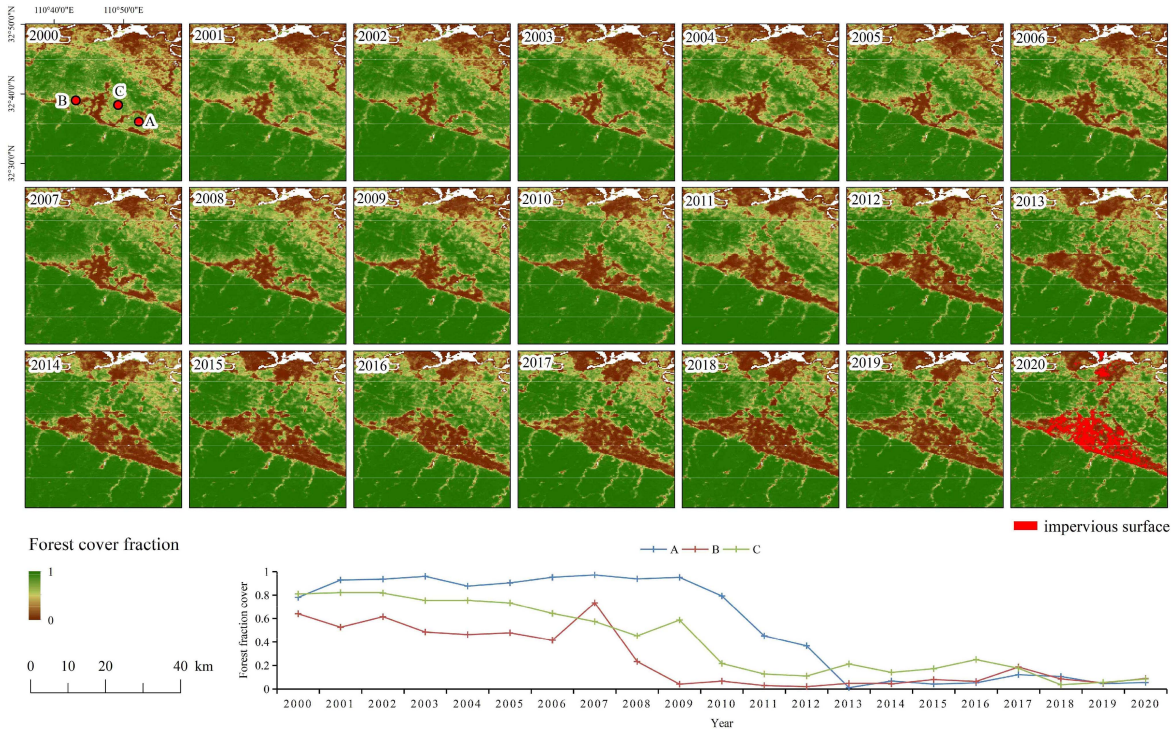

Fig. 8. Estimated annual forest cover fraction maps for the typical area of forest decrease in Shiyan City, Hubei Province.

fraction within the city increased, with an improved ecological environment around the city.

E. Annual Forest Cover Change During 2000–2020 at the Pixel Scale

In the above Section IV-B, the annual forest cover fraction maps for each year of the study area were obtained from 2000 to 2020, and this section analyzes the forest disturbances based on the results. Taking 0.5 as the segmentation threshold, pixels with forest cover fraction values greater than 0.5 are considered as forest cover pixels and assigned a value of 1, to obtain binary maps of forest cover in each year. The forest distribution maps were stacked based on the generated annual binary forest cover maps from 2000 to 2020. For a forest cover pixel in 2000, a forest cover decrease map was recorded for the year when the pixel first became a nonforest pixel. This operation was applied to all pixels to obtain a forest decrease change map in the study area. By contrast, a forest cover increase map was recorded for the year when the nonforest pixel at the beginning year of 2000 first became a forest pixel. The spatio-temporal information on forest cover change at the pixel scale in the study area can be understood through the obtained forest cover increase and decrease maps.

For the forest cover increase map [see Fig. 9(a)], it can be found that forest expansion in the study area is concentrated mainly in the vicinity of western Hanzhong city, central Ankang city, eastern Danjiangkou area, and southeastern Nanzhang and Baokang cities. Among them, the forest cover near the Danjiangkou Reservoir experienced a significant increase. This may be because the Danjiangkou Reservoir area belongs to the water source of the middle route of the South-to-North Water Diversion Project, which is a national first-class water source protection area, and the government has issued a strict forest protection policy for this region, such that relatively significant forest restoration was observed. Ankang city, as a representative area of forest restoration in Section IV-B, also showed a typical trend of forest restoration. A zoom of Ankang city area (see Ankang in Fig. 9) shows that the transformation of nonforest pixels to forest pixels occurred from the city boundaries to city center year-by-year. This indicates that more attention is paid to the development and protection of forest green space around the city in the process of urban construction.

From the forest cover decrease map [see Fig. 9(b)] it can be seen that a wide range of forest covers in 2000 became nonforests in the first years of the study period, which may be related to weak awareness of forest ecological protection in the early years. For example, the areas of continuous forest reduction in the study area are concentrated in the city center and some rural areas in the southeastern part. Taking Shiyan city as a zoomed area (see Shiyan in Fig. 9), it can be found that transformation of forest pixels to nonforest pixels occurs from city center to the city boundaries.

F. Effect of MODIS VCF Difference Threshold on Forest Cover Fraction Estimation

In Section III-C, the time-series MODIS VCF difference threshold a was used to determine whether a pixel is an unchanged sample in the predicting year [see (1) and (2)]. Based on this judgment, all constant, unchanged samples were selected

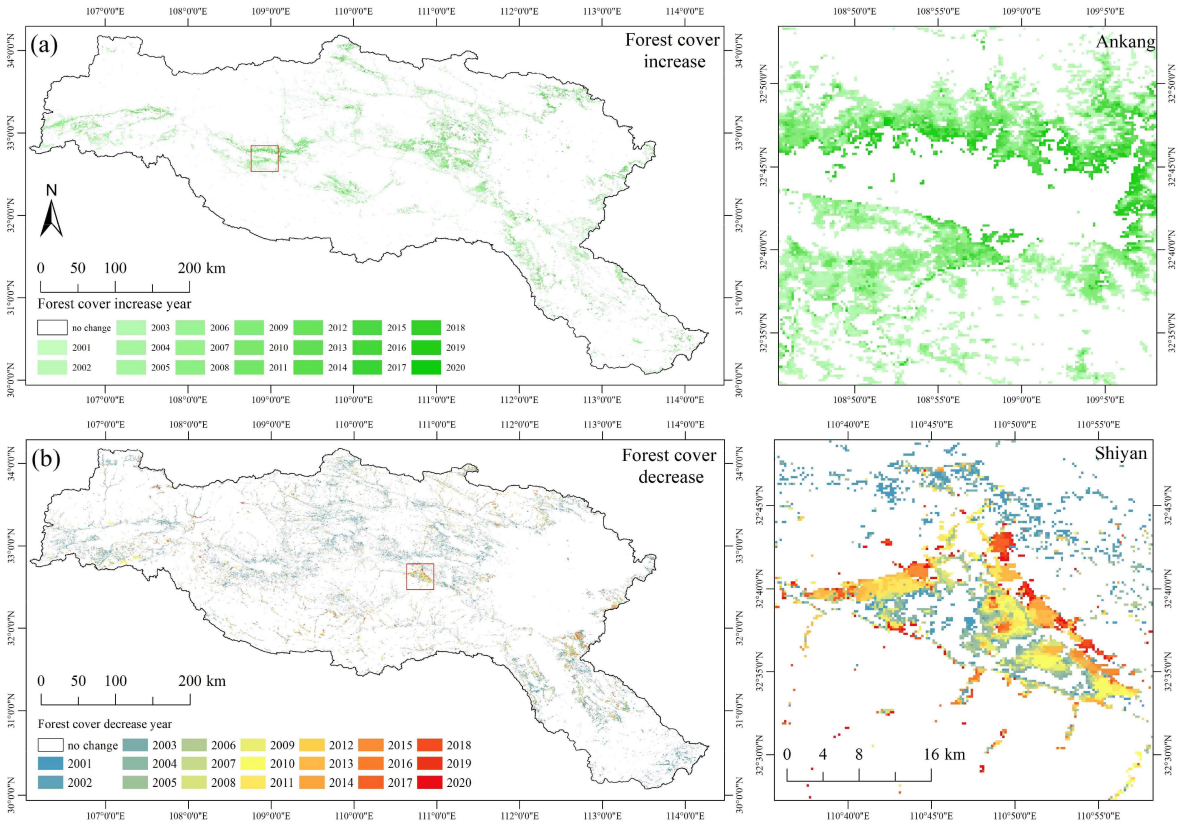

Fig. 9. Annual forest cover change during the period from 2001 to 2020 based on the baseline of the forest cover map for the year 2000 in China's Han River Basin. (a) Illustration of annual forest cover increase during 2001–2020, in which Ankang City, Shaanxi Province is used as a typical zoomed area of forest growth. (b) Illustration of annual forest cover decrease during 2001–2020, in which Shiyan City, Hubei Province is used as a typical zoomed area of forest decrease.

TABLE V
ACCURACY ASSESSMENT OF VARIOUS FOREST COVER FRACTION MAPS ESTIMATED BY STR WITH DIFFERENT MODIS VCF DIFFERENCE THRESHOLD VALUES IN (1)

	0.01	0.05	0.1	0.15	0.16	0.18	0.2	0.3
RMSE	0.1478	0.1386	0.1364	0.135	0.1351	0.1347	0.1349	0.1355
MAE	0.086	0.079	0.077	0.076	0.077	0.076	0.077	0.078
R^2	0.882	0.895	0.897	0.899	0.899	0.9	0.899	0.899
samples	1373	5231	7558	8615	8771	9039	9255	9809

from 2000 and 2020 for each predicting year and the MODIS NDVI sequence and annual MODIS VCF images of the predicting year were used together to estimate the forest cover fraction maps. As listed in Table V, this section analyzes the effect of the change in the MODIS VCF difference threshold a on forest cover fraction estimation, in which the combined samples of 2000 and 2020 were used in the proposed STR method.

When the threshold a is small (such as 0.01), although the screening requirement for unchanged samples is strict, the result of STR still presents an obvious improvement compared to the traditional RF method, in which the RMSE decreased from 0.1657 to 0.1478, MAE decreased from 0.1079 to 0.086, and R^2 increased from 0.851 to 0.882 (see Tables III and V). With a gradual increase in the threshold a, the number of selected unchanged training samples increases, which further increases the accuracy of the results. When a is increased to 0.18, relatively optimal results are obtained, with RMSE of 0.1347, MAE of 0.076, and R^2 of 0.9, as shown in Table V. However, with a continuous increase in the threshold a, the screening requirement for unchanged sample pixels becomes too lax, some low-quality samples will be included, and the accuracy of the result declines slightly, albeit still significantly better than the results obtained by the traditional RF method (see Table V). However, observing the change of sample size, it can be found that when a takes a relatively optimal value of 0.18, the sample size is nearly seven times than that of the sample size when a is 0.0. At the same time, when the value of a increases from 0.1 to 0.3, the sample size increases significantly, which increases the computational workload, but the accuracy of the obtained results does not increase significantly. Considering the tradeoff between accuracy and computational efficiency, we recommend a setting between 0.1–0.15 for a.

TABLE VI
EFFECT OF DIFFERENT W VALUES ON THE ACCURACY OF THE PREDICTED FOREST COVER FRACTION MAP IN 2019

Samples collection year			*RMSE*	*MAE*	R^2
2000	RF		0.2215	0.1292	0.792
	STR	*W*=1	0.1411	0.079	0.89
		W=3	0.1393	0.077	0.892
		W=5	0.1391	0.0771	0.893
		W=7	0.1389	0.0774	0.893
2020	RF		0.1621	0.1121	0.87
	STR	*W*=1	0.1384	0.081	0.895
		W=3	0.1379	0.079	0.895
		W=5	0.1375	0.0797	0.896
		W=7	0.1372	0.0798	0.896
2000+2020	RF		0.1657	0.1079	0.851
	STR	*W*=1	0.1366	0.0777	0.897
		W=3	0.1364	0.0774	0.897
		W=5	0.1364	0.0775	0.897
		W=7	0.1356	0.0772	0.898

G. Effect of Neighborhood Window System W on Forest Cover Fraction Estimation

In Section III-C, we believe that when the difference in MODIS VCF between two years is less than a given threshold, the pixel can be considered as an unchanged pixel. However, considering that MODIS VCF will inevitably have outliers caused by clouds and environmental condition changes, this will interfere with the operation of screening unchanged training samples. Therefore, we choose to build a neighborhood window system W instead of using a single pixel to indicate the change in percentage tree cover between two years. In this process, the different sizes of the neighborhood window system W will also have a certain impact on the prediction results. Therefore, we take 2019 as the predicted year and use different W values to quantify this impact.

By observing Table VI, it can be found that when $W = 1$ (i.e., only a single pixel is used for MODIS VCF change detection), the accuracy of the results obtained using the STR method is still significantly higher than that obtained by the traditional RF method, which once again demonstrates the effectiveness of the proposed STR method and the necessity of using MODIS VCF to select unchanged training samples. With the increasing of W, it can be found that the *RMSE* and *MAE* are reduced, and R^2 is also improved, which shows that the results can be further improved by constructing a neighborhood window system with larger W. However, considering that the increase in W value will also lead to a decrease in computational efficiency, W is, therefore, taken as 3 in this study.

H. Annual Forest Cover Fraction Change Trend During 2000–2020 Based on Mann–Kendall Trend Analysis

In this part, based on the annual forest cover fraction maps from 2000 to 2020 obtained in Section IV-B, the Mann–Kendall (M-K) trend analysis method was used here to analyze the forest cover fraction change trend in the study area, and the result is shown in Fig. 10. Since we are only interested the forest cover fraction change trends of forest areas, a nonforest mask was made to remove nonforest pixels in the trend map. In particular, the overlapped annual nonforest cover during 2000–2020 could be used as the nonforest mask required for this section, and we used 0.1 as the segmentation threshold when making a nonforest mask for each forest cover fraction map.

For the initial forest cover fraction change trend map shown in Fig. 10(a), the test statistic Z value obtained by M-K trend analysis was used to classify it as follows: 1) when $|Z| > 2.58$ (confidence level 99%), the change trend is extremely significant. 2) when $1.96 < |Z| < 2.58$ (confidence level 95%), the change trend is significant, otherwise the trend is insignificant. When Z value is positive, the change trend is increasing, and vice versa. The pie chart in Fig. 10(b) counts the percentage of pixels within different changing trends. Observing the statistical results of the pie chart in Fig. 10(b), there are 38% of the total pixels that have undergone significant changes, of which 27% have increased (of these, 18% of the pixels showed extreme increase, and 9% showed significant increase), accounting for 71% of the significantly changed pixels. However, only 11% of the pixels in the study area had a decrease trend (of these, 5% showed extreme decrease, and 6% showed significant decrease), which indicates that the overall trend of forest cover fraction in the study area is increasing. This conclusion is consistent with the change trend of the annual forest cover fraction maps (see Fig. 6) in Section IV-B.

From the spatial distribution of forest cover fraction trend in Fig. 10(a) and (b), it can be found that the forest cover fraction in many places have increased significantly from 2000 to 2020, such as the Hanzhong City in Shaanxi Province, Ankang City, and Danjiangkou area in Hubei Province, and Shangluo City in Shaanxi Province. By contrast, some areas experienced a forest fraction decrease trend during this period, such as Shiyan City and Yicheng City in Hubei Province in the southeast of the study area, which may be linked to the urban expansion during the past two decades. In the above annual forest cover increase and decrease maps obtained in Section IV-E, these areas

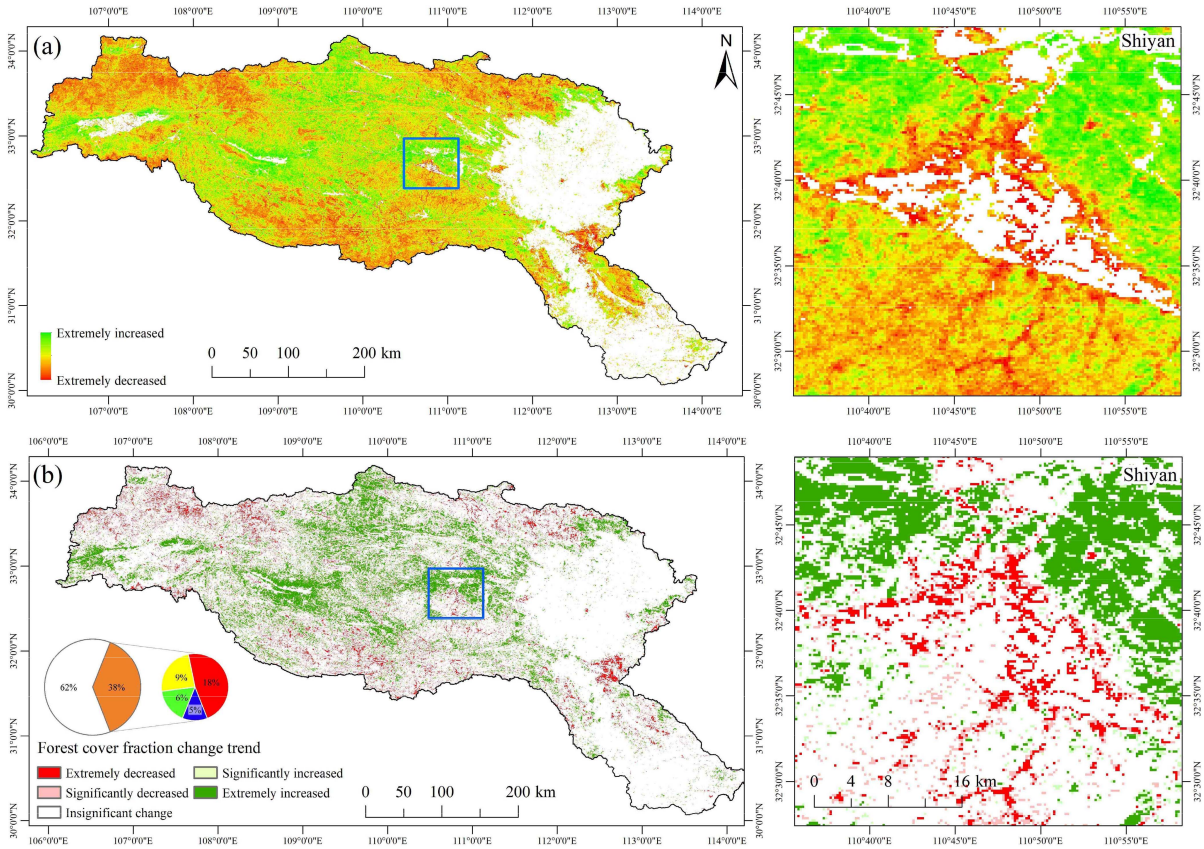

Fig. 10. Annual forest cover fraction change trend during the period from 2000 to 2020. (a) Forest cover fraction change trend map generated by Mann–Kendall trend analysis. (b) Classification of forest cover fraction change trend map according to different confidence levels, and the percentage of the number of pixels in different categories, in which Shiyan City, Hubei Province is used as a typical zoomed area.

also show similar typical forest cover changes. In addition, it is notable that the range of forest cover increase and decrease areas (see Fig. 10) obtained by M-K trend analysis is larger than that of the previous forest cover increase and decrease maps (see Fig. 9), this is because more subtle forest cover fraction changes can be observed in the trend map provided by M-K trend analysis. This also demonstrates the advantage of the annual forest cover fraction maps obtained by the proposed method in simultaneously tracking both high-intensity and low-intensity forest cover changes.

V. Discussion

A. Forest Cover Fraction Estimation With Reference Samples Extracted With Different Tree Height Thresholds

In Section III-B, the tree height threshold was used to convert the Landsat tree height images of 2000, 2019, and 2020 to Landsat binary forest cover maps, which were used to generate the reference 250 m forest cover fraction maps for these three years with a spatial averaging filter. It is noteworthy that different reference forest cover fraction maps generated from different tree height thresholds will lead to different results for the proposed STR method. The threshold of 5 m has been used widely to define a forest cover pixel [51], [59]. However, when land cover with a crown height greater than 10 m is regarded as forest, a new set of forest cover fraction maps from 2000 to 2020 will be obtained by STR. The forest cover fraction maps in 2000, 2010, and 2020 with tree height thresholds of 5 m and 10 m are shown in Fig. 11, where the Danjiangkou area is used as the zoomed area [see Fig. 10(g)–(l)].

From the results, it can be found that when the threshold is 10 m, the corresponding forest cover fraction values are significantly smaller than those with a threshold of 5 m. This is because the 10 m definition of forest is stricter than 5 m, and many young and low-quality forests in the study area will not be regarded as forest cover, and forest height is a good indicator for forest definition [60], [61]. In line with the trend of forest cover fraction maps obtained by the 5 m threshold, the forest composed of dominant tree species higher than 10 m were also recovered well by the proposed STR method during the study period, especially in the central region [see Fig. 11(d)–(f)]. This also shows that the STR method proposed can accurately reflect the temporal and spatial variation of the complex forest landscape in the Hanjiang River Basin according to the different definitions of forest height in the samples.

B. Forest Cover Fraction Change At Subpixel Scale

In Section IV-E, we made two annual forest cover change maps from the obtained forest cover fraction maps from 2000

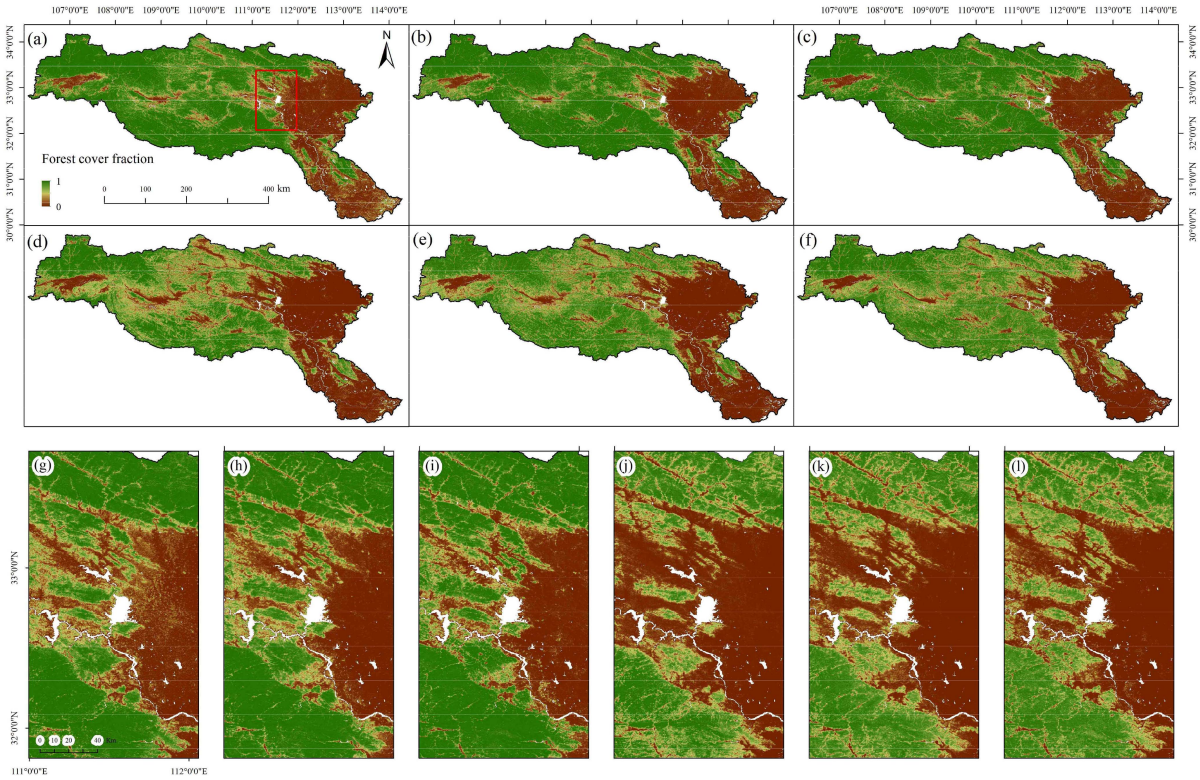

Fig. 11. Forest cover fraction maps estimated by STR with reference samples extracted with tree height thresholds of 5 m and 10 m. (a)–(c) Forest cover fraction maps in 2000, 2010, and 2020 after segmenting tree heights using a threshold of 5 m. (d)–(f) Forest cover fraction maps in 2000, 2010, and 2020 after segmenting tree heights using a threshold of 10 m. (g)–(i) Zoomed areas of (a)–(c); (j)–(l) Zoomed areas of (d)–(f).

to 2020 and analyzed the forest disturbances in the study area during the study period, but this is an analysis of forest cover change at the pixel scale. However, the forest cover fraction maps can also be used to analyze the changes to forests at the subpixel scale in any two time periods during the study period [28], [62]. In this part, the estimated forest cover fraction maps of the corresponding year were subtracted at 5-year intervals to obtain the forest cover fraction change for every five years of the study area, and the forest cover fraction of the start and end years was subtracted to obtain the forest cover fraction change for the entire study area over the past 21 years (see Fig. 12).

As shown in Fig. 12, from 2000 to 2005, the forest cover fraction in the western and eastern margins of the study area increased, and the southern and northern forests decreased to a certain extent [see Fig. 12(a)]. Between 2005 and 2010, there was obvious large area of forest recovery in the middle of the study area, and forest decline in the western and southeastern regions [see Fig. 12(b)]. From 2010 to 2015, forest recovery was more significant across the study area, and forest cover fraction increased in the western and central regions, especially around Hanzhong and Ankang cities, whereas forest decline continued in the east [see Fig. 12(c)]. Between 2015 and 2020, forests experienced an obvious decline in the south-central part and increased in the east and southeast [see Fig. 12(d)].

Examining the changes of forest cover fraction from 2000 to 2020 [see Fig. 12(e)], it can be seen that the increase in forest cover occurred mainly in the central, southeast central, and western edges of the study area. Although forest changes in the study area are also reflected in Section IV-E, Fig. 12(e) shows more low-intensity forest changes than the high-intensity changes that occurred at the pixel level in Fig. 9. Forest increases with low intensity were observed in the central and northern parts of the study area, with an increase of around 0.2 in the forest cover fraction, as well as the northwestern, southern, and southwestern parts of the study area. For the zoomed areas shown in Fig. 12(a1)–(e1) and (a2)–(e2), a significant decrease was observed in the central forests of the zoomed areas (a2)–(e2), and a decrease of low-intensity fraction cover can be found in the south, whereas a more significant increase occurred in the north.

C. Limitations and Future Research

The RF model was used as the nonlinear regression method in this study. In subsequent research, we will consider using many other machine learning methods, such as decision tree [63], naive Bayes [64], kernel logistic regression [65], support vector regression [66] for nonlinear regression, compare the performance of the different models, and then select the optimal model for the proposed STR method. At the same time, with an increase in the number of collected training samples, deep learning algorithms can automatically extract more useful features than machine learning algorithms [67], [68] and, thereby,

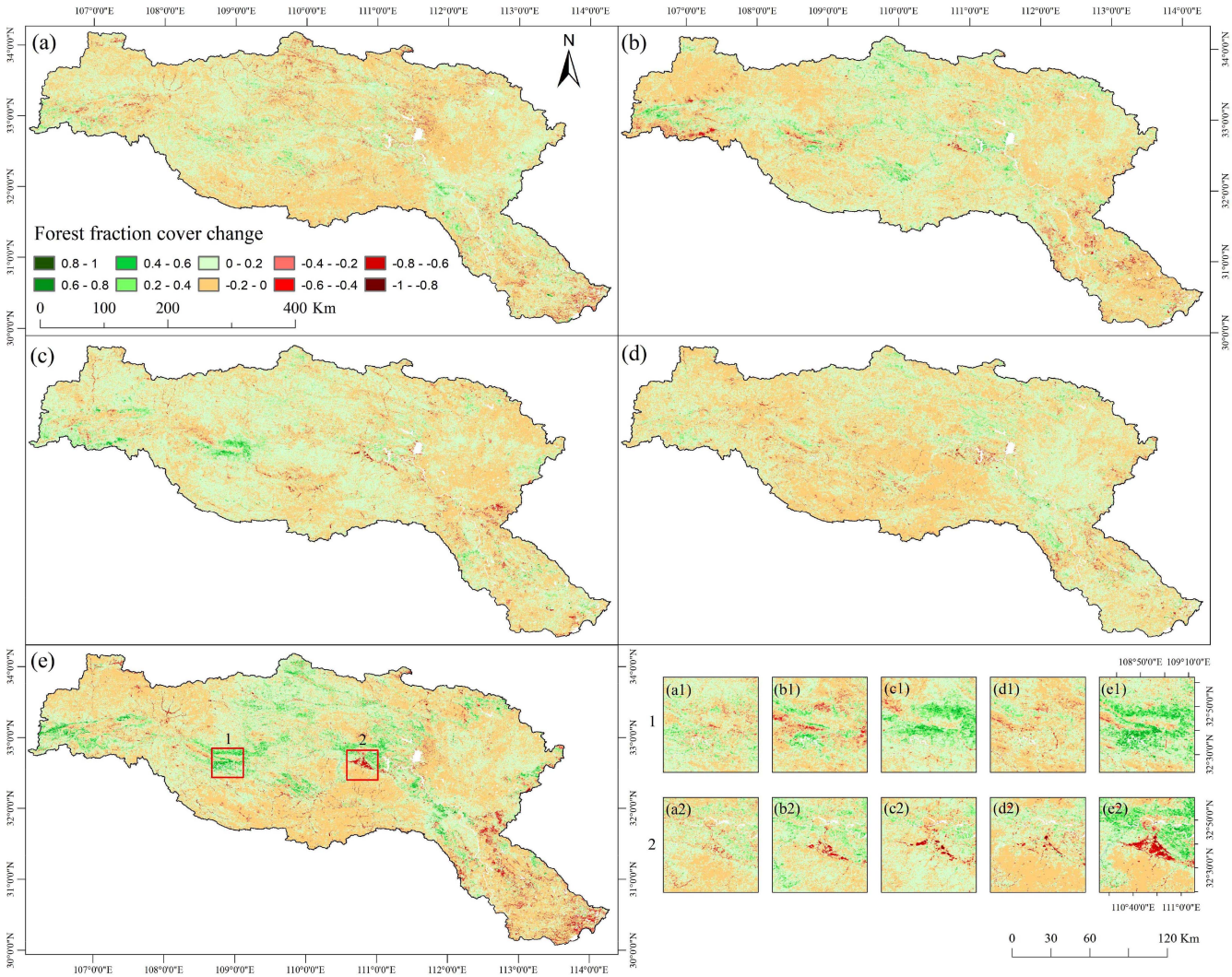

Fig. 12. Forest cover fraction change maps from 2000 to 2020 with an interval of five years. (a) Forest cover fraction change map between 2000 and 2005. (b) Forest cover fraction change map between 2005 and 2010. (c) Forest cover fraction change map between 2010 and 2015. (d) Forest cover fraction change map between 2015 and 2020. (e) Forest cover fraction change map between 2000 and 2020. (a1)–(e1) Zoomed areas of forest cover fraction change maps in (a)–(e) with a geolocation indicator of "1" in (e); (a2)–(e2) zoomed areas of forest cover fraction change maps in (a)–(e) with a geolocation indicator of "2" in (e).

increase the accuracy of forest cover fraction estimation. Although dynamics in MODIS VCF values can reflect changes in forest cover fraction to some extent, in practice, they cannot be completely positively correlated. In addition, MODIS VCF product itself has problems, such as misdetection of dense farmland areas, underestimation of sparse forests, and saturation of tree cover at around 80%. Therefore, uncertainty exists in the process of screening unchanged training samples in the proposed STR method by using the difference of time-series MODIS VCF images. In this research, to reduce the impact of uncertainty of MODIS VCF, we built a neighborhood window system W in Section III-C to select stable unchanged training samples. From the validation, we found generally that when the change of MODIS VCF values for a pixel between two years centered at a neighborhood window system W is less than a given threshold, the pixel has the same forest cover fraction value within two years, and the effectiveness of this principle has been demonstrated.

VI. Conclusion

The traditional nonlinear regression method is used to predict the forest cover fraction only at the acquisition time of training samples and is insufficient to estimate long time-series forest cover fraction. However, in practice, time-series forest cover fraction maps are crucial for the monitoring of spatio-temporal dynamics of forests, especially complex forest landscapes with varying environmental and climate conditions, such as in the Han River Basin, China. In this article, we proposed a new STR method that involves sample selection from a restricted span of two years to generate the necessary training data for each year between 2000 and 2020. Subsequently, the RF was employed to estimate time-serious forest cover fraction maps using the selected time-series training samples.

For the experiment based on the reference data in 2019 and tenfold cross validation, it showed that the proposed method can provide more accurate forest cover fraction maps than

traditional nonlinear regression. Taking the results obtained from the combined training samples in 2000 and 2020 as an example, after using the STR method, the RMSE changed from 0.1657 to 0.1364, which was 17.7% lower than before; MAE changed from 0.1079 to 0.077, with a decrease of 28.6% over the previous period; R^2 changed from 0.851 to 0.897, with an increase of 5%. The problems of overestimation and underestimation were also alleviated by STR. Moreover, this method can also reliably obtain high-quality results when predicting forest cover fraction maps far from the acquisition time of the training samples. Moreover, the forest cover fraction maps generated from GFCC in 2005, 2010, and 2015 were also used as reference data to further verify the effectiveness of the STR method. It is found that the proposed STR method can still obtain more accurate fraction cover maps than the traditional RF method by using this validation dataset. In addition, the impact of different neighborhood window system sizes on the prediction results of STR was also validated, and it can be found that better quality prediction results can be obtained after constructing a neighborhood window system.

By analyzing the generated annual forest cover fraction maps from 2000 to 2020, we concluded that the forests in the Han River Basin showed an overall recovery trend during the study period, in which Ankang City in Shaanxi Province presented a typical area of forest restoration, whereas the Shiyan City in Hubei Province depicted a typical forest decline due to urban expansion. At the same time, we analyzed the forest cover fraction changes at the subpixel scale, and many low-intensity forest cover fraction changes were found. With different threshold values of 5 m and 10 m in training sample generation, it was found that the proposed STR method can accurately reflect the spatiotemporal changes of complex forest landscapes. In future research, alternative machine learning models will be compared to select the model with the best performance.

ACKNOWLEDGMENT

The authors would like to thank NASA LP DAAC at the USGS EROS Center for providing free MODIS NDVI and MODIS VCF. The authors would also like to thank the Global Land Analysis and Discovery Lab at the University of Maryland for providing the GLAD Global Forest Canopy Height dataset.

REFERENCES

[1] R. Pilli and A. Pase, "Forest functions and space: A geohistorical perspective of European forests," *Iforest-Biogeosci. Forestry*, vol. 11, no. 1, pp. 79–89, Feb. 2018.

[2] M. C. Hansen et al., "High-resolution global maps of 21st-century forest cover change," *Science*, vol. 342, no. 6160, pp. 850–853, 2013.

[3] N. L. Harris et al., "Global maps of twenty-first century forest carbon fluxes," *Nature Clim. Change*, vol. 11, no. 3, pp. 234–240, 2021.

[4] J. A. Foley et al., "Global consequences of land use," *Science*, vol. 309, no. 5734, pp. 570–574, Jul. 2005.

[5] R. Seidl et al., "Forest disturbances under climate change," *Nature Clim. Change*, vol. 7, no. 6, pp. 395–402, 2017.

[6] Y. Zhang et al., "Tracking small-scale tropical forest disturbances: Fusing the Landsat and Sentinel-2 data record," *Remote Sens. Environ.*, vol. 261, 2021, Art. no. 112470.

[7] Y. Zhang et al., "Monitoring monthly tropical humid forest disturbances with Planet NICFI images in Cameroon," *Agricultural Forest Meteorol.*, vol. 340, 2023, Art. no. 109676.

[8] E. G.-Ampadu and M. Gebreslasie, "Two decades progress on the application of remote sensing for monitoring tropical and sub-tropical natural forests: A review," *Forests*, vol. 12, no. 6, Jun. 2021, Art. no. 739.

[9] G. V. Lui and D. A. Coomes, "A comparison of novel optical remote sensing-based technologies for forest-cover/change monitoring," *Remote Sens.*, vol. 7, no. 3, pp. 2781–2807, Mar. 2015.

[10] S. Francini et al., "Near-real time forest change detection using PlanetScope imagery," *Eur. J. Remote Sens.*, vol. 53, no. 1, pp. 233–244, Jan. 2020.

[11] V. G.-Jaramillo et al., "Assessment of deforestation during the last decades in Ecuador using NOAA-AVHRR satellite data," *Erdkunde*, vol. 70, no. 3, pp. 217–235, Jul.–Sep. 2016.

[12] R. M. Lucas et al., "Mapping the regional extent of tropical forest regeneration stages in the Brazilian Legal Amazon using NOAA AVHRR data," *Int. J. Remote Sens.*, vol. 21, no. 15, pp. 2855–2881, Oct. 2000.

[13] J. G. Masek et al., "United States forest disturbance trends observed using Landsat time series," *Ecosystems*, vol. 16, no. 6, pp. 1087–1104, Sep., 2013.

[14] R. J. Frazier, N. C. Coops, and M. A. Wulder, "Boreal Shield forest disturbance and recovery trends using Landsat time series," *Remote Sens. Environ.*, vol. 170, pp. 317–327, Dec. 2015.

[15] J. Reiche et al., "Forest disturbance alerts for the Congo Basin using Sentinel-1," *Environ. Res. Lett.*, vol. 16, no. 2, Feb. 2021, Art. no. 024005.

[16] S. Ganz, P. Adler, and G. Kändler, "Forest cover mapping based on a combination of aerial images and Sentinel-2 satellite data compared to national forest inventory data," *Forests*, vol. 11, no. 12, 2020, Art. no. 1322.

[17] X. X. Zhu et al., "Estimation of the restored forest spatial structure in semi-arid mine dumps using Worldview-2 imagery," *Forests*, vol. 11, no. 6, Jun. 2020, Art. no. 695.

[18] L. Wang et al., "Comparison of IKONOS and QuickBird images for mapping mangrove species on the Caribbean coast of Panama," *Remote Sens. Environ.*, vol. 91, no. 3–4, pp. 432–440, Jun., 2004.

[19] W. H. Qi et al., "Forest restoration efforts drive changes in land-use/land-cover and water-related ecosystem services in China's Han River basin," *Ecol. Eng.*, vol. 126, pp. 64–73, Jan. 2019.

[20] X. Wang, Y. H. Zhang, and K. R. Zhang, "Automatic 10 m forest cover mapping in 2020 at China's Han River Basin by fusing ESA Sentinel-1/Sentinel-2 Land cover and Sentinel-2 near real-time forest cover possibility," *Forests*, vol. 14, no. 6, Jun. 2023, Art. no. 1133.

[21] R. Singh et al., "Forest disturbance detection in Garhwal Himalayas using MODIS NDVI time-series and BFAST model," *Geocarto Int.*, vol. 37, no. 26, pp. 12689–12708, Dec. 2022.

[22] Y. Gao et al., "Monitoring forest disturbance using time-series MODIS NDVI in Michoacan, Mexico," *Geocarto Int.*, vol. 36, no. 15, pp. 1768–1784, Sep. 2021.

[23] J. Yao et al., "Monitoring responses of forest to climate variations by MODIS NDVI: A case study of Hun River upstream, Northeastern China," *Eur. J. For. Res.*, vol. 131, no. 3, pp. 705–716, 2012.

[24] Y. Qin et al., "Annual dynamics of forest areas in South America during 2007–2010 at 50-m spatial resolution," *Remote Sens. Environ.*, vol. 201, pp. 73–87, 2017.

[25] L. Busetto, M. Meroni, and R. Colombo, "Combining medium and coarse spatial resolution satellite data to improve the estimation of sub-pixel NDVI time series," *Remote Sens. Environ.*, vol. 112, no. 1, pp. 118–131, Jan. 2008.

[26] K. Jia et al., "Forest cover classification using Landsat ETM+ data and time series MODIS NDVI data," *Int. J. Appl. Earth Observ. Geoinf.*, vol. 33, pp. 32–38, 2014.

[27] J. Y. Yang et al., "Extraction of multiple cropping information at the sub-pixel scale based on phenology and MODIS NDVI time-series: A case study in Henan Province, China," *Geocarto Int.*, vol. 37, no. 27, pp. 15999–16019, Dec. 2022.

[28] Y. H. Zhang et al., "Mapping annual forest cover by fusing PALSAR/PALSAR-2 and MODIS NDVI during 2007-2016," *Remote Sens. Environ.*, vol. 224, pp. 74–91, Apr. 2019.

[29] Q. Wang, X. Ding, X. Tong, and P. M. Atkinson, "Real-time spatiotemporal spectral unmixing of MODIS images," *IEEE Trans. Geosci. Remote Sens.*, vol. 60, 2022, Art. no. 5404816.

[30] X. Ding, Q. Wang, and X. Tong, "Integrating 250 m MODIS data in spectral unmixing for 500 m fractional vegetation cover estimation," *Int. J. Appl. Earth Obs. Geoinf.*, vol. 111, 2022, Art. no. 102860.

[31] D. A. Roberts et al., "Mapping Chaparral in the Santa Monica Mountains using multiple end member spectral mixture models," *Remote Sens. Environ.*, vol. 65, no. 3, pp. 267–279, 1998.
[32] R. Tateishi, Y. Shimazaki, and P. D. Gunin, "Spectral and temporal linear mixing model for vegetation classification," *Int. J. Remote Sens.*, vol. 25, no. 20, pp. 4203–4218, 2004.
[33] D. Lu et al., "Fractional forest cover mapping in the Brazilian Amazon with a combination of MODIS and TM images," *Int. J. Remote Sens.*, vol. 32, pp. 7131–7149, Nov. 2011.
[34] C. Tottrup et al., "Mapping fractional forest cover across the highlands of mainland Southeast Asia using MODIS data and regression tree modelling," *Int. J. Remote Sens.*, vol. 28, no. 1, pp. 23–46,2007.
[35] X. Liu et al., "Mapping 30 m fractional forest cover over China's Three-North Region from Landsat-8 data using ensemble machine learning methods," *Remote Sens.*, vol. 13, 2021, Art. no. 2592.
[36] M. O. Sarif, C. Jeganathan, and S. Mondal, "MODIS-VCF based forest change analysis in the State of Jharkhand," *Proc. Nat. Acad. Sci. India Sect. A-Phys. Sci.*, vol. 87, no. 4, pp. 751–767, Dec. 2017.
[37] Y. Gao et al., "Assessing forest cover change in Mexico from annual MODIS VCF data (2000-2010)," *Int. J. Remote Sens.*, vol. 39, no. 22, pp. 7901–7918, 2018.
[38] M. C. Hansen et al., "A method for integrating MODIS and Landsat data for systematic monitoring of forest cover and change in the Congo Basin," *Remote Sens. Environ.*, vol. 112, no. 5, pp. 2495–2513, 2008.
[39] F.-J. Liu et al., "Assessment of the three factors affecting Myanmar's forest cover change using Landsat and MODIS vegetation continuous fields data," *Int. J. Digit. Earth*, vol. 9, no. 6, pp. 562–585, 2016.
[40] M. Boschetti et al., "Multi-year monitoring of rice crop phenology through time series analysis of MODIS images," *Int. J. Remote Sens.*, vol. 30, no. 18, pp. 4643–4662, 2009.
[41] E. Yan et al., "Phenology-based classification of vegetation cover types in Northeast China using MODIS NDVI and EVI time series," *Int. J. Remote Sens.*, vol. 36, no. 2, pp. 489–512, 2015.
[42] D. Chu et al., "Long time-series NDVI reconstruction in cloud-prone regions via spatio-temporal tensor completion," *Remote Sens. Environ.*, vol. 264, 2021, Art. no. 112632.
[43] J. C. D. Oliveira, J. C. Epiphanio, and C. D. Rennó, "Window regression: A spatial-temporal analysis to estimate pixels classified as low-quality in MODIS NDVI time series," *Remote Sens.*, vol. 6, no. 4, pp. 3123–3142, 2014.
[44] J. Chen et al., "A simple method for reconstructing a high-quality NDVI time-series data set based on the Savitzky-Golay filter," *Remote Sens. Environ.*, vol. 91, no. 3–4, pp. 332–344, 2004.
[45] F. Li et al., "Urban vegetation phenology analysis using high spatio-temporal NDVI time series," *Urban For. Urban Greening*, vol. 25, 2017, Art. no. 57.
[46] O. Cartus et al., "Large area forest stem volume mapping in the boreal zone using synergy of ERS-1/2 tandem coherence and MODIS vegetation continuous fields," *Remote Sens. Environ.*, vol. 115, no. 3, pp. 931–943, Mar. 2011.
[47] M. C. Hansen et al., "Global percent tree cover at a spatial resolution of 500 meters: First results of the MODIS vegetation continuous fields algorithm," *Earth Interact.*, vol. 7, no. 10, pp. 1–15, 2003.
[48] M. C. Hansen et al., "Humid tropical forest clearing from 2000 to 2005 quantified by using multitemporal and multiresolution remotely sensed data," *Proc. Natl. Acad. Sci. USA*, vol. 105, no. 27, pp. 9439–9444, Jul. 2008.
[49] M. Simard et al., "Mapping forest canopy height globally with spaceborne lidar," *J. Geophys. Res.: Biogeosci.*, vol. 116, 2011, Art. no. G4.
[50] P. Potapov et al., "Mapping global forest canopy height through integration of GEDI and Landsat data," *Remote Sens. Environ.*, vol. 253, 2021, Art. no. 112165.
[51] P. Potapov et al., "The global 2000-2020 land cover and land use change dataset derived from the Landsat archive: First results," *Front. Remote Sens.*, vol. 3, 2022, Art. no. 856903.
[52] F. Oloo, G. Murithi, and C. Jepkosgei, "Quantifying tree cover loss in urban forests within Nairobi City metropolitan area from Earth observation data," *Environ. Sci. Proc.*, vol. 3, 2021, Art. no. 78.
[53] J. O. Sexton et al., "Global, 30-m resolution continuous fields of tree cover: Landsat-based rescaling of MODIS vegetation continuous fields with lidar-based estimates of error," *Int. J. Digit. Earth*, vol. 6, no. 5, pp. 427–448, 2013.
[54] N. L. Harris et al., "Baseline map of carbon emissions from deforestation in tropical regions," *Science*, vol. 336, no. 6088, pp. 1573–1576, 2012.
[55] L. Breiman, "Random forests," *Mach. Learn.*, vol. 45, no. 1, pp. 5–32, 2001.
[56] D. R. Cutler et al., "Random forests for classification in ecology," *Ecology*, vol. 88, no. 11, pp. 2783–2792, 2007.
[57] V. F. R.-Galiano et al., "An assessment of the effectiveness of a random forest classifier for land-cover classification," *ISPRS J. Photogramm. Remote Sens.*, vol. 67, pp. 93–104, 2012.
[58] L. T. H. Pham and L. Brabyn, "Monitoring mangrove biomass change in Vietnam using SPOT images and an object-based approach combined with machine learning algorithms," *ISPRS J. Photogramm. Remote Sens.*, vol. 128, pp. 86–97, 2017.
[59] M. C. Hansen et al., "Humid tropical forest disturbance alerts using Landsat data," *Environ. Res. Lett.*, vol. 11, no. 3, Mar. 2016, Art. no. 034008.
[60] W. Li et al., "High-resolution mapping of forest canopy height using machine learning by coupling ICESat-2 LiDAR with Sentinel-1, Sentinel-2 and Landsat-8 data," *Int. J. Appl. Earth Obs. Geoinf.*, vol. 92, 2020, Art. no. 102163.
[61] H. Huang, C. Liu, and X. Wang, "Constructing a finer-resolution forest height in China using ICESat/GLAS, Landsat and ALOS PALSAR data and height patterns of natural forests and plantations," *Remote Sens.*, vol. 11, no. 15, 2019, Art. no. 1740.
[62] C. Senf et al., "A generalized regression-based unmixing model for mapping forest cover fractions throughout three decades of Landsat data," *Remote Sens. Environ.*, vol. 240, 2020, Art. no. 111691.
[63] K. Liu et al., "Monitoring mangrove forest changes using remote sensing and GIS data with decision-tree learning," *Wetlands*, vol. 28, pp. 336–346, 2008.
[64] M. Li, J. Im, and C. Beier, "Machine learning approaches for forest classification and change analysis using multi-temporal Landsat TM images over Huntington wildlife forest," *GISci. Remote Sens.*, vol. 50, no. 4, pp. 361–384, 2013.
[65] S. I. Elmahdy et al., "Spatiotemporal mapping and monitoring of mangrove forests changes from 1990 to 2019 in the Northern Emirates, UAE using random forest, kernel logistic regression and naive Bayes tree models," *Front. Environ. Sci.*, vol. 8, 2020, Art. no. 102.
[66] A. Okujeni et al., "Support vector regression an and synthetically mixed training data for quantifying urban land cover," *Remote Sens. Environ.*, vol. 137, pp. 184–197, Oct. 2013.
[67] K. N. Trong and H. T. Xuan, "Coastal forest cover change detection using satellite images and convolutional neural networks in Vietnam," *IAES Int. J. Artif. Intell.*, vol. 11, no. 3, pp. 930–938, 2022.
[68] K. Isaienkov et al., "Deep learning for regular change detection in Ukrainian forest ecosystem with sentinel-2," *IEEE J. Sel. Topics Appl. Earth Observ. Remote Sens.*, vol. 14, pp. 364–376, 2021.

Xinyan Zhong received the B.Sc. degree in surveying and mapping engineering from the School of Geodesy and Geomatics, Wuhan University, Wuhan, China, in 2021. She is currently working toward the Ph.D. degree in physical geography with the Innovation Academy for Precision Measurement Science and Technology, Chinese Academy of Sciences, Wuhan, and also with the University of Chinese Academy of Sciences, Beijing, China.

Her research interests focus on forest change monitoring.

Yun Du received the B.S. degree in geomorphology and quaternary geology from Nanjing University, Nanjing, China, in 1989, the M.S. degree in physical geography from the Institute of Geodesy and Geophysics, Chinese Academy of Sciences, Wuhan, China, in 1992, and the Ph.D. degree in historical geography from Wuhan University, Wuhan, in 1999.

He is currently a Professor with Innovation Academy for Precision Measurement Science and Technology, Chinese Academy of Sciences. His research interests include environment monitoring and evaluation.

Xia Wang received the B.S. and M.S. degrees in land resource management from the China University of Geosciences, Wuhan, China, in 2012 and 2014, respectively, and the Ph.D. degree in land resource management from Wuhan University, Wuhan, in 2018.

From 2021 to 2022, she was a Visiting Scholar with the Lancaster Environment Centre, Faculty of Science and Technology, Lancaster University, Lancaster, U.K. From 2018 to 2022, she was a Lecturer with the School of Environmental Ecology and Biological Engineering, Wuhan Institute of Technology. Since 2022, she is an Assistant Researcher with Wuhan Botanical Garden, Chinese Academy of Sciences, Beijing, China. Her research interests include the field of ecological environment assessment and environmental remote sensing monitoring.

Xiaodong Li received the B.S. degree in geographic information system from China University of Geosciences, Wuhan, China, in 2006, and the M.S. and Ph.D. degrees in physical geography from the Institute of Geodesy and Geophysics, Chinese Academy of Sciences, Wuhan, in 2009 and 2012, respectively.

He is currently a Professor with the Innovation Academy for Precision Measurement Science and Technology, Chinese Academy of Sciences. He has been supported by the Youth Innovation Promotion Association of the Chinese Academy of Sciences and Hubei Province Natural Science Fund for Distinguished Young Scholars. His research interests include superresolution mapping and fusion of remotely sensed imagery.

Wenqiong Zhao received the B.S. degree in geographic information science from China University of Geosciences, Wuhan, China, in 2023. He is currently working toward the master's degree in physical geography with the Innovation Academy for Precision Measurement Science and Technology, Chinese Academy of Sciences, Wuhan, and also with the University of Chinese Academy of Sciences, Beijing, China.

His research interests include forest mapping of remotely sensed imagery and remote sensing applications in ecology resources.

Yihang Zhang received the B.S. degree in land resource management from China University of Geosciences, Wuhan, China, in 2012, and the Ph.D. degree in physical geography from the Institute of Geodesy and Geophysics, Chinese Academy of Sciences, Wuhan, in 2017.

From 2015 to 2016, he was a Visiting Ph.D. Student under the supervision of P. M. Atkinson with the Lancaster Environment Centre, Faculty of Science and Technology, Lancaster University, Lancaster, U.K. From 2021 to 2023, he was a Postdoctoral Fellow with the Lancaster Environment Centre joint supported by Lancaster University and CSC. He has been supported by the Young Top-notch Talent Cultivation Program of Hubei Province, the Hubei Province Natural Science Fund for Distinguished Young Scholars, and the Yellow Crane Talent Program of Wuhan. He is currently an Associate Professor with Innovation Academy for Precision Measurement Science and Technology, Chinese Academy of Sciences, Beijing, China. His research interests include global forest cover mapping, spatio-temporal fusion, and downscaling of remotely sensed imagery.

Peter M. Atkinson received the Ph.D. degree in geography from the University of Sheffield, Sheffield, U.K., in 1990, and the MBA degree in management from the University of Southampton, Southampton, U.K., in 2012.

He was a Professor of geography with the University of Southampton, where he is currently a Visiting Professor. He is currently a Distinguished Professor of spatial data science and the Dean with the Faculty of Science and Technology, Lancaster University, Lancaster, U.K. He is also a Visiting Professor with the Chinese Academy of Sciences, Beijing, China. He has authored and coauthored more than 300 peer-reviewed articles in international scientific journals and around 50 refereed book chapters. He has also edited nine journal special issues and eight books. His research interests include remote sensing, geographical information science, and spatial (and space-time) statistics applied to a range of environmental science, and socio-economic problems.

Dr. Atkinson was the recipient of the Peter Burrough Award of the International Spatial Accuracy Research Association and the NERCCASE award with Rothamsted Experimental Station. He is Editor-in-Chief of *Science of Remote Sensing*, a sister journal of *Remote Sensing of Environment*. He also sits on the editorial boards of several further journals including *Geographical Analysis*, *Spatial Statistics*, and *Environmental Informatics*. He was the Belle van Zuylen Chair with Utrecht University, The Netherlands. He is a Fellow of the Learned Society of Wales.